AD727179

FIRST ANNUAL TECHNICAL REPORT

RESEARCH ON AMORPHOUS MATERIALS

June 1, 1970 - May 31, 1971

Contract DAHC04 70 C 0044

DDC
RECEIVED
AUG 1971
A

The views and conclusions contained in this document are those of the authors and should not be interpreted as necessarily representing the official policies, either expressed or implied, of the Advanced Research Projects Agency or the U. S. Government.

DISTRIBUTION STATEMENT A
Approved for public release;
Distribution Unlimited

CMR-71-11

Reproduced by
NATIONAL TECHNICAL
INFORMATION SERVICE
Springfield, Va. 22151

CENTER FOR MATERIALS RESEARCH

STANFORD UNIVERSITY • STANFORD, CALIFORNIA

BEST
AVAILABLE COPY

FIRST ANNUAL TECHNICAL REPORT

June 1, 1970 - May 31, 1971

Sponsored by
Advanced Research Projects Agency
ARPA Order No. 1562

Program Code Number: 0D10

Contractor: Stanford University

Contract No. DAHC04 70 C 0044

Principal Investigators: W. E. Spicer
Phone (415) 321-2300, Ext. 4643

A. Bienenstock, Ext. 2617

R. H. Bube, Ext. 2535

Effective Date of Contract: June 1, 1970

Contract Expiration Date: May 31, 1971

Amount of Contract: $84,605

Contract Title: RESEARCH ON AMORPHOUS MATERIALS

CENTER FOR MATERIALS RESEARCH
STANFORD UNIVERSITY
STANFORD, CALIFORNIA 94305
(415) 321-2300, Ext. 4118

TABLE OF CONTENTS

ILLUSTRATIONS

ILLUSTRATIONS (Cont)

TABLES

INTRODUCTION

This report describes our first year's efforts to study some of the relationships among structure, bonding, electronic structure and transport properties of various amorphous semiconductors. The organization of this report is quite different from that of the report describing the first six months' work. In that report, it seemed most appropriate to divide the material into those areas supervised by the three principal investigators. At the present time, such a division is rather difficult because of the large number of cooperative and joint efforts. It has proved valuable to move in directions in which particular materials are prepared and studied jointly, with different areas of expertise coordinated towards common goals of understanding. Hence, we have chosen to organize the report in terms of increasing complexity of materials being studied.

The report begins, therefore, with studies of elemental amorphous materials. It goes on to a description of our efforts with binary materials and ends with an account of research on more complex systems.

To those searching out the most important results, we summarize those as follows.

1. Continued research on amorphous Ge and Si tends to reinforce the basic results that these materials are best described by a random network model in which there are, in some cases, voids. Contrary to most theoretical models, however, the best samples of these materials do not show high density tails in the electronic densities of states. This work is described in Section I of the report.

2. Starting with x-ray diffraction radial distribution studies, and then continuing with neutron diffraction, x-ray induced photoemission, x-ray absorption edge spectroscopy and ultraviolet photoemission, it has been shown that the bonding in the Ge-Te amorphous alloy system is quite different from that in crystalline GeTe. The studies rule out the possibility that amorphous GeTe can be described as microcystalline GeTe. They show that the bonding is considerably more covalent than in crystalline GeTe or, for that matter, crystalline GeSe or GeS. These experimental results, taken together, present the strongest structural confirmation of the Mott-Cohen, Fritzsche and Ovshinsky model of bonding in amorphous semiconductors. This work is described in Sections II.B through II.F of the report.

3. It has been demonstrated that the addition of metallic dopants to amorphous As_2Se_3 markedly suppresses infrared absorption associated with small concentrations of oxygen. When taken together with the results of other workers, this result implies that the judicial use of such dopants may considerably simplify infrared window technology. This work is described in Section III.A of the report.

4. Considerable progress has been made towards the development of a model which may explain most of the photoconductive properties of complex amorphous chalcogenide alloys. This work is described in Section III.B.

I. ELEMENTAL MATERIALS

This section is concerned with studies of the closely related elemental amorphous materials, Si and Ge. It consists of three parts. The first is a brief study of an important approximation in a paper which is generally accepted as having shown that amorphous Si is best described by a random network model with, in certain cases, voids. The second portion is a preprint describing photoemission measurements on amorphous Ge which relate electronic densities of states to deposition and annealing conditions. In addition, this work establishes the position of the Fermi level at the surface. In the third section, speculations about the relationship between measured electronic properties and the void structure are presented. A tentative attempt is made to understand the differences in the densities of states for the crystalline and amorphous materials in terms of the covalent bond and the Bragg reflection conditions.

A. Structural Studies (F. Betts and A. Bienenstock)

The question of whether the structures of amorphous materials are best described by a microcrystalline or random network model has been with us now for nearly forty years. It takes on added importance in a period when scientists are attempting to understand charge transport in them, for each model would dictate a different interpretation of the low conductivities.

In recent years, however, there appears to be a strong shift in favor of the random network type models for amorphous semiconductors. The strongest case provided is that by Betts et al[1] for amorphous GeTe, where no crystalline analogue is apparent, as discussed above. In addition, however, the work of Moss and Graczyk[2] presents strong evidence for the inapplicability of the microcrystalline model to amorphous silicon. These authors obtained careful electron diffraction data on the material. They then calculated the diffraction pattern to be expected from a variety of microcrystalline models and showed that none of the calculations could yield the measured intensities. A potential shortcoming of their work was that they neglected to include the effects of intercrystallite scattering in their calculations. That is, they assumed that each crystallite scatters independently. The justification for this neglect was uncertain.

The difficulty of assessing the role of interparticle interference comes from the fact that no one has a clear idea of how the crystallites would be arranged in a microcrystalline array of the high packing fractions necessary to achieve amorphous densities. To circumvent this problem and obtain an estimate of the order of magnitude of the interparticle

interference terms, we have approximated the microcrystalline system with a rather simple model.

The model assumes, first of all, that there is no correlation in the orientation of neighboring crystallites. This may be its most serious flaw. Nevertheless, it does allow for considerable simplification of the mathematics and should give reasonable order of magnitude results.

The second assumption of the model is that the probability of finding two crystallites separated by a given distance is given by the Finney[3] radial distribution function for the "liquid" packing of hard spheres.

Finally, we note that in using the hard sphere radial distribution, it is necessary to ascribe a hard sphere radius to the microcrystallites. If one uses a radius characteristic of the crystallite size, it is apparent that the high density of amorphous silicon will not be achieved. Hence, we have adjusted the hard sphere radius in the pair distribution function to match the density. This implies that some crystallites overlap.

Under these three approximations, we have calculated the effects of interparticle interference for the most important of the models considered by Moss and Graczyk and found them to be negligible at all but very small angles, where our approximations are unreliable. Since the discrepancies between the model calculations and the observed intensities are most important at higher angles, our calculations indicate that it is extremely unlikely that the discrepancies can be explained on the basis of interparticle interference. Hence, they provide added support for a random network model of amorphous silicon.

1. F. Betts, A. Bienenstock and S. R. Ovshinsky, J. Non-Cryst. Solids 4, 554 (1970).

2. S. C. Moss and J. F. Graczyk, Phys. Rev. Letters 23, 1167 (1969).

3. J. L. Finney, Ph.D. Thesis, University of London. (The detailed radial distribution function was supplied by private communication.)

B. Photoemission Investigation of Amorphous Germanium*

C. G. Ribbing† D. T. Pierce and W. E. Spicer

ABSTRACT: Photoemission measurements of amorphous germanium films have been made in the photon energy range 6.2-11.7 eV. A spectrum with one broad peak 1.25 eV below the high energy cutoff is obtained, similar to earlier results of Spicer and Donovan. By comparison with gold spectra and using simple models for the resolution function and the high energy edge in the electron distribution, the valence band edge is placed 0.31 ±0.05 eV below the Fermi-energy, with no evidence for tailing of the density of states into the gap. Careful annealing measurements through several temperatures below the crystallization temperature showed no gradual changes until the rather abrupt appearance of crystalline structure after anneals to 300 and 350° C. Deposition at rates of 2 Å/sec. and 26 Å/sec. gave no significant change nor did deposition onto substrates at -170° to +150° C. The absolute photoelectric yield was measured and it's energy dependence found to be in very good agreement with recent theoretical results of Ballantyne. During successive annealings the yield first increased and then decreased to a significantly smaller value than the amorphous yield. A tentative explanation of this behavior is given within a random network description of amorphous germanium.

I. INTRODUCTION

The electronic structure of amorphous germanium films has been intensively studied during recent years. Important contributions have been the theoretical work of Mott[1,2], the optical and electrical measurements by Clark[3], the optical studies of Tauc et al[4-6], the photoemission and optical measurements by Spicer and Donovan[7-9], and the very recent studies of optical properties and their dependence on annealing and deposition rate by Thèye[10,11].

In the work reported here, which is an extension and refinement of the photoemission measurements of Spicer and Donovan, we particularly wanted to study how the annealing properties of amorphous Ge films varied with deposition conditions such as substrate temperature and evaporation rate. We also aimed to locate the Fermi level with respect to the valence band edge. Since there has been considerable discussion[6] about tailing of the density of states into the gap, we also considered it worthwhile to repeat Spicer and Donovan's[9] comparison of photoelectron energy distribution curves (EDC's) for amorphous Ge with the EDC's of the same film annealed in situ until characteristic crystalline structure appeared.

II. EXPERIMENTAL

The measurements were performed with UV-light monochromated to a full width at half maximum of 0.10-0.20 eV over a photon energy range $6.2 \leq \hbar\omega \leq 11.8$eV. The upper limit was set by the transmission cutoff of the LiF-window on the ultra high vacuum chamber. The photoelectron energy was measured with the spherical screened emitter retarding field energy analyzer described by DiStefano and Pierce[12,13]. The energy distribution curves were obtained using the ac modulation technique reported by Spicer and Berglund[14] and Eden[15].

The substrate holder was essentially a block of annealed copper which could be pivoted out of the collector so that the substrate was in a horizontal position for evaporation. The substrate was a polished disk shaped single crystal of Ge (p-type, 11 Ωcm, from Semimetal). The substrate holder contained a heater and a thermocouple used to monitor the sample temperature.

A special cooling device was constructed which allowed the sample to be cooled to near liquid nitrogen temperature. It consisted principally of a 15 cm long, 5 mm thick flexible bundle of hydorgen fired 0.013 mm OFHC copper wires, the ends of which were brazed into blocks of annealed copper. One block was tightly screwed onto the tip of a cold-finger that could be filled with liquid nitrogen from the outside of the chamber. The other end was connected to the substrate holder via a polished sapphire disc 1 mm thick, providing good thermal conduction to the substrate, but also electrical insulation from the chamber. An extra pyrex washer had the effect of increasing the mechanical pressure between disc and substrate when the metal parts thermally contracted. This way of cooling does not give quite as low a final temperature as cooling the substrate directly with liquid nitrogen, but the extra noise due to the vibrations from the boiling liquid is avoided. A test showed that with this set-up we could change the sample temperature from -170° C to +600° C both in the emission and evaporation positions.

After roughing, bake out and pump down to ultrahigh vacuum (UHV), the substrate was heat cleaned at more than 450° C for about 15 minutes, and the e-gun and source material was outgassed by pre-evaporation with the shutter closed. The evaporations were made with an e-gun 48 cm from the substrate. The material used was intrinsic grade polycrystalline Ge obtained from

Eagle-Picher. The rate of deposition and the final film thickness were monitored with a quartz microbalance mounted next to the substrate. All films studied in this work were about 1000 Å thick. During the evaporations the chamber base pressure of 1×10^{-10} Torr rose to 7×10^{-9} Torr for a deposition rate of 2 Å/sec. The higher deposition rate of 26 Å/sec increased the pressure to 1×10^{-7} Torr.

III. RESULTS AND DISCUSSION

Comparison to Previous Experiment

An EDC from a film evaporated onto a room temperature (RT $\cong$ 293° K) substrate at a rate of 2 Å/sec is compared in Fig. 1 to an EDC measured by Spicer and Donovan.[9] While there is general overall agreement, the two noticeable differences in our EDC are the 0.25 eV shift of the main peak to higher energy and the extra, very weak structure 3 eV below the main peak. We attribute the shift of the main peak to the improved resolution obtained using the screened energy analyzer[12]. We locate the position of the main peak 1.25 eV below the valence band edge. The new structure is too weak for us to conclude whether or not it is due to a real increase in the initial density of states. It appears just as probable that it originates from a superposition of scattered electrons onto the bottom of the valence band. This weak shoulder is visible through several photon energies, 10.2 to 11.7 eV, at about the same position relative to the main peak. When the measurements on this film were repeated at a sample temperature of -170° C, a sharpening of the leading edge of about 0.08 eV was observed at lower photon energies. We attribute this shift to a reduced electron-phonon scattering.

Location of the Valence Band Edge

A difficult problem in photoemission studies of semiconductors is to place the high energy cutoff properly, thereby locating the valence band edge. The cutoff in the semiconductor is caused by the density of states and is not so steep as the metallic cutoff due to the Fermi function at RT. Also, since the edge is broadened by the instrumental resolution function, it is necessary to somehow deconvolve the experimental curve to find the true cutoff in the density of states. (We shall use the concept of resolution function, meaning the experimental curve obtained from measuring an emitted δ-function distribution. Effectively, it is the same as the conventional "window" in ordinary spectroscopy, only with the opposite shift in non-symmetric cases.)

In order to find the valence band edge in amorphous Ge we have used the following procedure based on comparison with the cutoff for a metal. The EDC's of Au films were recorded in the same geometry and at the same low photon energies as the Ge films. Taking the metallic cutoff as the midpoint of the linear part of the high energy edge gave a total width of the EDC which was in excellent agreement with the difference between the photon energy and work function of the collector as determined independently by a Fowler plot of the yield. Such a cutoff in the middle of the high energy edge indicates that the resolution function is symmetric as can be seen from the idealized case in Fig. 2 a and b. A symmetric (case 1) and non-symmetric (case 2) resolution function are shown in Fig. 2a where the arrows symbolize the emitted δ-function distribution of electrons. The non-symmetric resolution function of case 2 shifts the edge to lower energy and hence shifts the cutoff away from the middle of the linear region. Since imperfect analyzer geometry gives a non-symmetric resolution function

as in case 2, we suggest that this error is unimportant compared to random errors such as an unevenness in the analyzer work function and the spectral line width of the UV-light. The principal reason for the insignificant geometrical error is probably the screened emitter analyzer.

In order to get a quantitative description, the two simple models of a rectangular and triangular resolution function are treated in Fig.2c-f. The true emitted density of states in the metal is assumed to be broadened only by the Fermi function which we approximate by a straight edge like the dotted distribution in Fig. 2c. This model neglects the curvature of the Fermi function close to 0 and 1, but since we are only going to use the straight middle part of the edges in our analysis we consider this to constitute a reasonable first approximation. By convolving[16] the rectangular resolution function with the true distribution (dotted line) we obtain the measured distribution (full line). The measured EDC will have a linear region with a corresponding interval L_m on the E-axis. The relation, $L_m = W - x_m$ where W is the width of the resolution function and x_m the width of the true distribution, is easily found. To determine the instrumental constant W it remains to decide what width x_m should be attributed to the metal like distribution. This is done either by merely plotting the room temperature Fermi function or by using the first order expansion $f(E) = \frac{1}{2}[1-(E-E_f)/2kT]$ and extrapolating to $f(E) = 0$ and 1. In both cases, at 20° C a value of $x_m = 0.10$ eV ($\cong 4kT$) is obtained. L_m is determined from the measured Au EDC's to be 0.15 eV with good reproducibility through several low photon energies. We conclude from the Au measurements and from an analysis of these simple models that the resolution function is symmetric with a width $W = 0.25$ eV.

For comparison, the effect of a triangular window is shown in Fig. 2e. The same overall effect of this convolution is observed, i.e. rounding off corners and leaning the edge back. The rectangular resolution function was chosen for the analysis of the experimental results since it appears to give marginally better agreement with the experimental shape and is simpler to convolve.

A striking feature in the experimental EDC's from the amorphous Ge is that their leading edges also have a linear part. This indicates that the true distribution has a linear region of at least the same length. We take as the simple model for the semiconductor case a linear edge as represented by the dashed line in Fig. 2d. The difference from the "metallic" edge is that the slope is considerably less steep and the true cutoff is at the end of the edge. Fig. 2d shows the result of convolving this edge with the same resolution function as in Fig. 2c. Two observations should be made: a large linear region is obtained in the middle of the edge, and, as is to be expected when the resolution function has a smaller width than the measured structure, the slope of the edge is retained in that linear region. For the semiconductor, the relation between the linear edge and the width of the resolution function is $L_{sc} = x_{sc} - W$. The location of the true cutoff is W/2 higher than the end of the linear region, which coincides with the extrapolation of the linear part to the E-axis. It is not practical to relate anything to the cutoff of the instrumentally boadened EDC since the high energy "foot" is disturbed by noise and zero line drift. Again for comparison, the effect of a triangular resolution function on the same edge is demonstrated in Fig. 2f. This model appears to exaggerate the linearity of the experimental edge.

The application of the analysis above to recorded curves of Au and Ge is shown in Fig. 3. Average values of $L_{sc} = 0.29$ and $x_{sc} = 0.54$ eV are found. The valence band edge is placed $0.31 \pm .05$ eV below the Fermi level by measurements from several EDC's at different low photon energies. The extrapolation of the linear part of the edge is in all cases in very close agreement tothe cutoff obtained in this analysis which shows the consistency of our simple models with the experimental results.

Results from Annealed Films

The amorphous films obtained by evaporation were all annealed in successive steps by raising the substrate temperature for about one hour to a predetermined value and remaining at that temperature for half an hour. A precision of $\pm 5^{\circ}$ C was usual. The dramatic effect of heat treatment at 300° C and above is demonstrated in Fig. 4. The broad structureless EDC of the amorphous material is transformed into the rich structure typical for crystalline Ge. After the final photoemission experiment it was furthermore verified by x-ray diffraction that the film gave (220) diffraction peaks that were not present on the other side of the (111)-oriented substrate. From the width of the diffraction peaks the size of the crystallites was estimated to be 200-300Å .

Again the qualitative agreement with the annealing experiment of Spicer and Donovan[8] is satisfactory, but there is a shift in the crystallization temperature. Structure characteristic of crystalline film is apparent in our EDC's after annealing at $250\text{-}300^{\circ}$ C and is fully developed after annealing at $300\text{-}350^{\circ}$ C. The corresponding temperature interval for the Ge films of Donovan and Spicer are $300\text{-}400^{\circ}$ C and $400\text{-}450^{\circ}$ C respectively, and the EDC's display a more gradual change. There still remains some

uncertainty about the source of these differences. Adamski[17] has shown experimentally that the amorphous to polycrystalline and polycrystalline to epitaxial transformation temperatures are very sensitive to oxygen partial pressures as low as 5×10^{-9} Torr during evaporation. Nowick[18] also argues that the presence of any impurities that are insoluble in the crystalline phase stabilizes the amorphous phase. Crystallization would force such impurities to separate out in a second phase which corresponds to a high activation energy. The 1×10^{-11} Torr base pressure quoted by Spicer and Donovan is better than ours, so the only apparent source of extra oxygen in their experiment is their higher pressure during evaporation, 1×10^{-7} Torr as compared to our 7×10^{-9} Torr. We note however that the poorer vacuum with their high evaporation rate discussed below did not affect the crystallization temperature. The preparation of the crystalline substrates, polishing and later heat cleaning in high vacuum, was virtually identical in both experiments so approximately the same amounts of substrate oxides were probably present initially.

As was originally noted by Spicer and Donovan the high energy edge of the EDC's for amorphous Ge is at least as sharp as for polycrystalline Ge. In fact the crystalline edge is somewhat less steep, which can be understood as an effect of parabolic bands. It should be noted, however, that photoemission alone cannot rule out the possibility of a very small density of states in the gap $\sim 10^{17} cm^{-3}$, as reported by Tauc, Menth and Wood[19] for amorphous As_2S_3.

A striking feature of Fig. 4 is the similarity between the EDC's from films heated only up to 250°C. This result is different from the recent results of Thèye[10] who observes a gradual change in refractive index and

absorption coefficient for annealing temperatures well below the crystallization temperature (400° C). Thèye attributes this change to unsatisfied bonds which decrease in number when the film is annealed. We believe that these unsatisfied bonds are surface states on micro-voids as demonstrated for amorphous Si by Moss and Graczyk[20]. Arguing against the presence of micro-voids, Thèye claims that her films showed no decrease in density when annealed. A decrease, however, should only occur if the voids migrated to the surface, but not if they merely coalesced and thereby reduced the void surface and the number of "dangling bond".

Independent of what the defects are that cause the gradual changes upon annealing in Thèye's films, it seems as if they are not present in our films. A shift in the absorption edge of about 0.4 eV (Fig. 4, Ref. 10) would show up in the EDC's unless all the shift was due to a change in the final density of states below the vacuum level, an assumption that appears rather artificial. The obvious reason for the absence of defects should then be the several orders of magnitude lower base pressure in our case. Thèye's high deposition rate almost makes up for the quoted 10^{-6} Torr evaporation pressure from the point of view of contamination. The fact that the crystallization temperature however was 100° C higher than ours seems to indicate the presence of more impurities[17,18] as discussed above. The importance of Thèye's work therefore is that it demonstrates that it is possible by careful annealing to approach "the perfect amorphous state" obatinable directly in ultrahigh vacuum. In view of these experiences it is tempting to speculate that the controversy[3,6,7,21] about tailing in the density of states into the forbidden gap is caused by different preparation techniques giving rise to more or less voids[23] in the film.

The amount of voids is substantially reduced if the film is deposited under clean conditions in ultra-high vacuum.

Recently it has been noted by Donovan[22] and Spicer that Ge typically evaporates in the forms Ge_1, Ge_2, Ge_3, and Ge_4 and that the composition of the material striking the substrate could effect the characteristics of amorphous films so formed. One would expect the "perfect" amorphous film to be most closely approached when Ge arrives at the substrate as separated atoms. Low evaporation temperatures and long evaporation distances should maximize this since the fraction of atomic Ge is highest at low temperatures and since as the evaporation distance is increased, the probability of Ge_2, Ge_3, or Ge_4 breakup to produce more atomic Ge is increased. We did not check this hypothesis but we consider it to be a possible explanation for the discrepancies reported in the literature on the properties of amorphous germanium.

Effect of Substrate Temperature

In subsequent evaporations the effect of different substrate temperatures was investigated. This is exemplified for the substrate temperatures -170, 20, 150, and 260° C in Fig. 5. The slight broadening of the 150° C curve is most likely due to the fact that it was recorded with a conventional diode analyzer rather than with the screened emitter analyzer. We find it a rather remarkable verification of the well-defined properties of amorphous Ge that the EDC's varied so little over a range in substrate temperature as large as 320° C.

Apparently, the 260° C substrate temperature was just as effective to crystallize the material as a 300° C anneal. This is easy to understand, as pointed out by Nowick[18], from the fact the mobility required for crystal-

lization is easier to obtain on a free surface during an evaporation than in the already built up film. The films evaporated at the three lower temperatures all crystallized in the same 250-350° C range in contrast to the observation of Thèye[11], who reports a lower crystallization temperature the higher the substrate temperature. Tentatively, we suggest that this discrepancy is due to the larger amount of voids in Thèye's films. The voids in the imperfect amorphous film impede crystallization, but they are reduced in number when the substrate is heated due to the higher surface mobility of the impinging atoms.

The object of the 260° C evaporation was to see if the high density form of amorphous Ge, reported by Donovan et al[23], had some characteristic feature in photoemission. Due to the lower crystallization temperature this question remains to be answered. In principle the high density phase could have been formed on the 150° C. substrate, but in such a case the same EDC's were obtained as in the case of the normal density amorphous film.

Effect of Rate of Deposition

To investigate what influence the evaporation rate could have on the EDC's of amorphous Ge, one evaporation was tried with as high rate as was possible within the constraints of the long source to substrate-distance and the desire to maintain a pressure $\leq 1 \times 10^{-7}$ Torr. A rate of 26 Å/sec was recorded. This is far from the 200 Å/sec reported by Thèye[10,11], but it was hoped that any gross effect of deposition rate would be revealed by the increase from 2 to 26 Å/sec. A pressure of 1×10^{-7} Torr during an evaporation of more than 30 sec. corresponds to a maximum contamination of 1 to 2 monolayers of gas molecules over the 1000 Å of the film. Therefore, it is not

conclusively demonstrated that the shift to lower energy of the main peak and the broadening of the high energy edge in Fig. 5 really stems from the high evaporation rate. The possibility of contamination cannot be ruled out.

The Photoelectric Yield

The yield of photoemitted electrons per incident photon was measured over the entire energy range using a calibrated Cs_3Sb photocell[24] and a +45 V bias on the collector. The absolute yield was calculated using the formula $Y = y/(1-R)T$ where y is the yield found from measurement, R is the reflectivity of the film and T is the transmission of the LiF window. Since no reflectivity data for fine grain polycrystalline films was available we chose to use reflectivity data for amorphous Ge.

The resulting yields for amorphous and annealed film are presented in Fig. 7. At high energies the yield of the amorphous film is between the yield of the film annealed at 300 and 450° C. We believe that this surprising result can be interpreted in the following way. Assuming that our amorphous Ge forms an ideal or almost ideal tetrahedral random network[25], it is easily conceived that the thermal scattering is higher than in a single crystal with long range order. This will give the amorphous film a higher yield since increased probability of elastic or almost elastic scattering will increase the probability that an excited electron reaches the escape cone[26]. This arguement is based on the assumption that the electron-electron scattering length is larger than the defect scattering length. The first annealing step to 300° C can then be understood as breaking up the network and creating small crystallites ($\lesssim$200 Å). The large amount of internal surface barriers will <u>increase</u> the total scattering giving rise

to the higher yield obtained. Continued annealing to 350-450° C increases the grain size which will reduce the scattering and thus the yield in complete qualitative agreement with the results in Fig. 7. The choice of amorphous reflectivity data cannot be responsible for this effect, since reflectance values reported[27] for crystalline Ge would make the yield for the 450° C annealed film even lower by as much as 25% at 11 eV. It could, however, make the difference between the amorphous and the 300° C annealed film much smaller. It can be remarked that this behavior of the yield through annealing would be very difficult to reconcile with any kind of microcrystalline model where the annealing process has to be conceived as a successive growth of microcrystallites.

Attempts to fit the energy dependence of the yield for the amorphous film to any simple power law[28] failed, even for energy ranges close to threshold. Very recent results of Ballantyne[29], however, gave a remarkably good fit over a range of almost 3 eV as seen in Fig. 8. The energy dependence of the yield derived by Ballantyne for the case of a rectangular energy distribution of excited electrons is: $Y \propto (h\nu - \varphi)^3/(h\nu)^2$ where $h\nu$ is the photon energy and φ is the threshold. The derivation of this formula includes a smearing out of the rectangular distribution by a phenomenologidal scattering against phonons, defects, impurities or surfaces. The extrapolated value for the threshold is found to be 4.98 ± .04 eV in good agreement with the sum of the values for the work function 4.63 ±.04eV and the difference in energy between Fermi level and valence band maximum 0.31 ± 0.05 eV that were obtained from the EDC's.

Acknowledgements

The authors would like to thank Prof. Joe Ballantyne for giving us

access to his results prior to publication and for several valuable comments. We would like to thank Dr. Terry Donovan for providing the reflectivity data for amorphous geranium as well as for several informative discussions. We also want to express our appreciation of the endurance and skill displayed by Phil McKernan in constructing the cooling device.

* This work was supported by the Advanced Projects Agency through Army Office of Scientific Research and through the Center for Material Science at Stanford University.

† On a grant from the Swedish Board for Technical Development.

References

1. N. F. Mott, Adv. In Physics, 16, 49 (1967)
2. N. F. Mott, Phil. Mag., 19, 835 (1968)
3. A. H. Clark, Phys. Rev. 154, 750 (1967)
4. J. Tauc, R. Grigrovici, A. Vancu, Phys. Status Solidi 15, 627 (1966)
5. J. Tauc, Mat. Res. Bull. 3, 37 (1968)
6. J. Tauc, A. Abraham, R. Zallen, M. Slade, J. Noncryst. Solids 4, 279 (1970)
7. T. M. Donovan, W. E. Spicer, Phys. Rev. Lett 22,:20, 1058 (1969)
8. W. E. Spicer, T. M. Donovan, Phys. Rev. Lett. 24: 11, 595 (1970)
9. W. E. Spicer, T. M. Donovan J. of Non-cryst. Solids 2, 66 (1970)
10. M. L. Thèye, Nat. Res. Bull. 6: 2, 103 (1971)
11. M. L. Thèye, to be published.
12. T. DiStefano, D. Pierce, Rev. Sci. Instr. 41, 180 (1970)
13. D. Pierce, T. DiStefano, Rev. Sci. Instr. 41, 1740 (1970)
14. W. E. Spicer, C. N. Berglund, Rev. Sci. Instr. 35, 1665 (1964)
15. R. C. Eden, Rev. Sci. Instruments. 41, 252 (1970)
16. E. A. Guillemin, Theory of Linear Physical Systems, Chap. 13, J. Wiley 1963
17. R. F. Ademsky J. of Appl. Phys. 40, 4301 (1969)
18. A. S. Nowick, Comments on Solid State Physics V2, 155 (1970)
19. J. Tauc, A Menth, D. L. Wood, Phys. Rev Lett. 25, 749 (1970)
20. S. C. Moss, J. F. Greczyk, Phys. Rev. Lett. 23, 1167 (1969)
21. J. W. Osmun, H. Fritzsche, Appl. Phys. Lett. 16, 87 (1970)
22. T. Donovan, private communication
23. T. M. Donovan, E. J. Ashley, W. Spicer, Phys. Lett. 32A, 85 (1970)
24. R. Y. Koyama, thesis, Tech. Rep. #5223-1, appendix 1, Stanford (1969)

25. D. E. Polk, J. of Non Cryst. Solids. 5, 365 (1971)

26. R. N. Stuart, F. Wooten, Phys. Rev. 156, 364 (1967)

27. H. R. Philipp, H. Ehrenreich, Phys. Rev. 129, 1550 (1963)

28. E. O. Kane, Phys. Rev. 127, 131 (1962)

29, J. Ballantyne, to be published

Figure-Captions

Fig. 1 A comparison of amorphous Ge EDC's of Spicer and Donovan (ref 9) and of the present work showing the 0.25 eV shift of the main peak and the extra low energy structure 3 eV below the main peak.

Fig. 2 Convolution of linear edges with model resolution functions:

a) symmetric and non-symmetric rectangular resolution functions.

b) the effect of convolving a step-shaped edge with the resolution functions in (a) showing the shift of the edge in a non-symmetric case.

c) "Metallic" case, showing the convolution of a rectangular distribution function with a linear edge of smaller width.

d) "Semiconductor" case convolving a rectangular distribution function with a linear edge of larger width.

e) Like (c) but with a triangular resolution function.

f) Like (d) but with a triangular resolution function.

Fig. 3 Location of the valence band edge of amorphous germanium using EDC's from Ge and Au recorded in the same geometry.

Fig. 4 The effect of annealing on the EDC's of amorphous Ge films. The curves are normalized to the absolute photoelectric yield.

Fig. 5 The effect of different substrate temperatures on the EDC's of Ge films. The 150° C curve was recorded with a conventional diode analyzer.

Fig. 6 Two normalized EDC's of Ge films deposited on RT substrate at different rates.

Fig. 7 The absolute photoelectric yield for an as deposited Ge film,

after a 300° C anneal and after a 450° C anneal.

Fig. 8 The photoelectric yield of amorphous Ge fitted to the relation of Ref. 28.

Figure 1

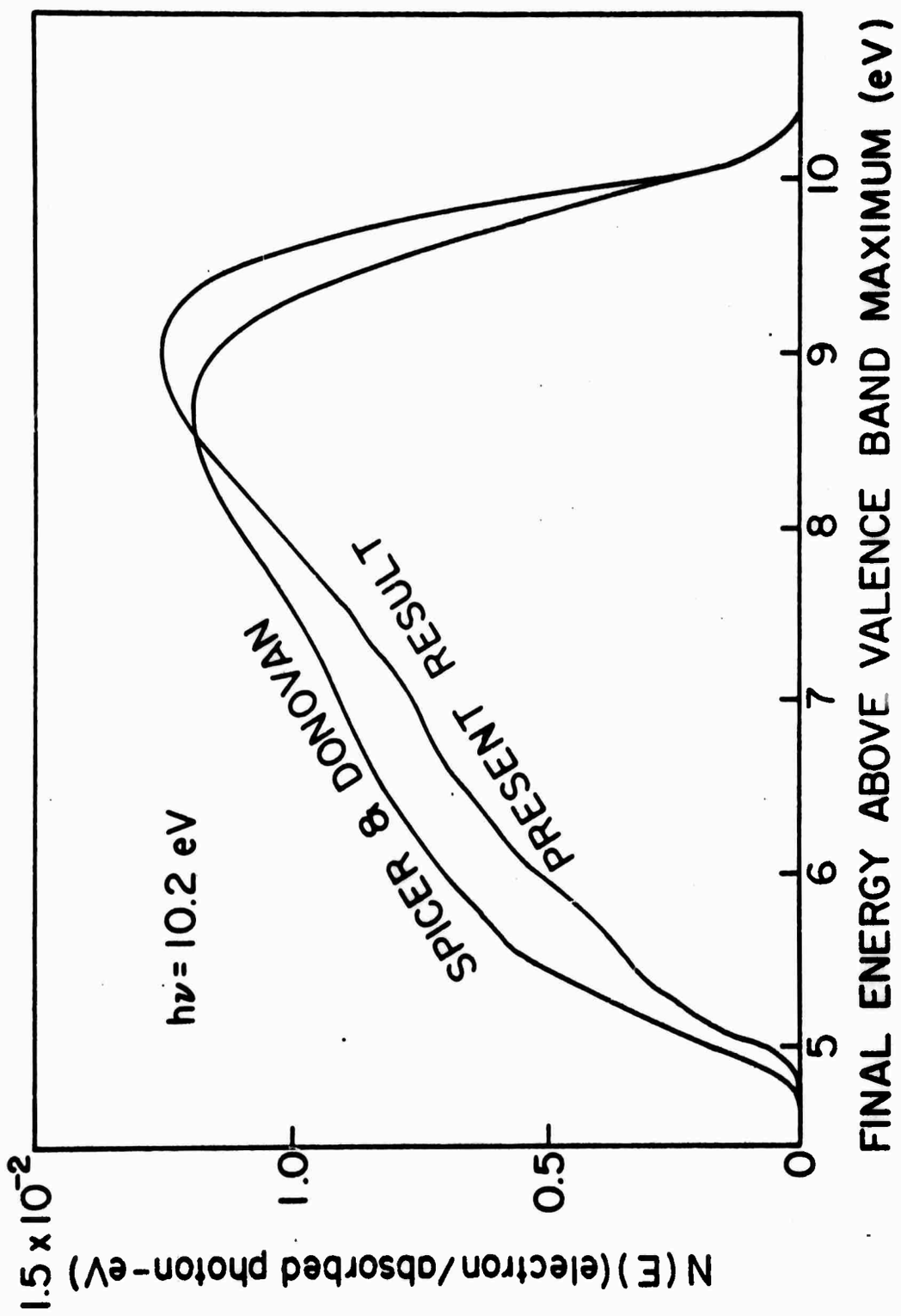
N (E) (electron/absorbed photon-eV)
1.5 x 10⁻²
1.0
0.5
0
5
6
7
8
9
10
FINAL ENERGY ABOVE VALENCE BAND MAXIMUM (eV)
hν = 10.2 eV
SPICER & DONOVAN
PRESENT RESULT

Figure 2

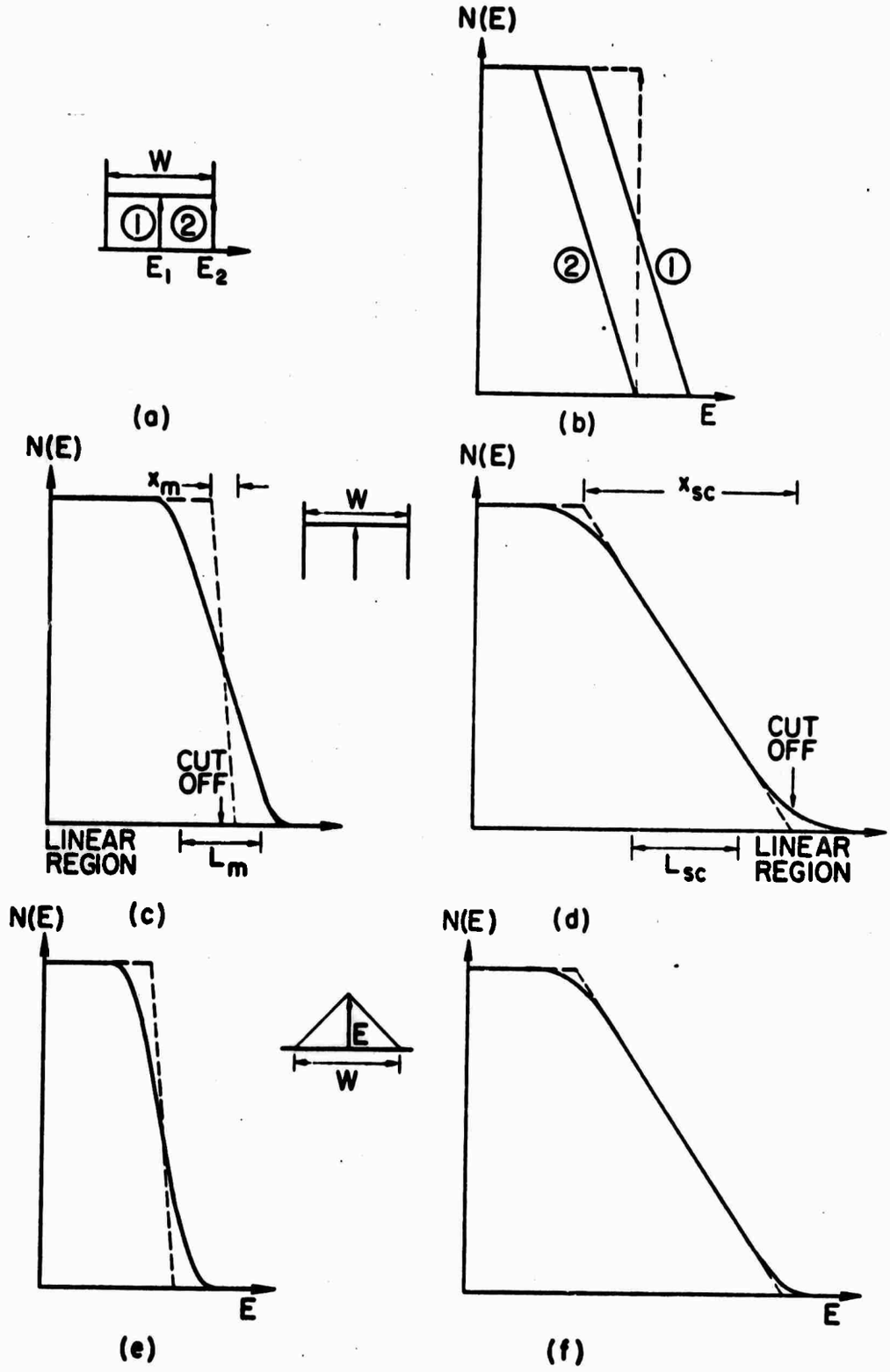
N(E)
W
①
②
E1
E2
(a)
②
①
(b)
E
N(E)
xm
W
CUT
OFF
LINEAR
REGION
Lm
N(E)
xsc
CUT
OFF
Lsc
LINEAR
REGION
N(E)
(c)
E
W
E
(e)
N(E)
(d)
E
(f)

Figure 3

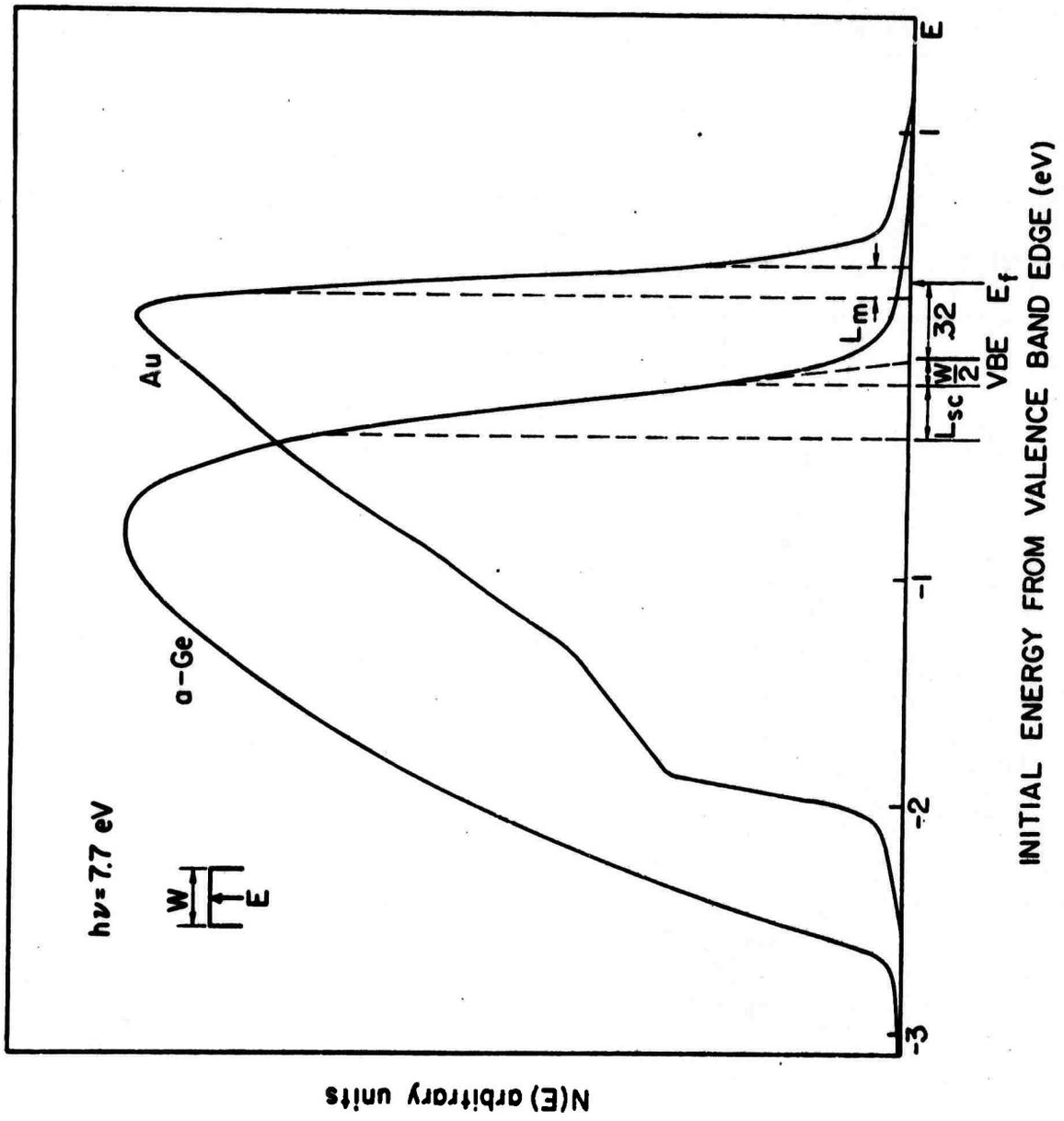
N(E) arbitrary units
INITIAL ENERGY FROM VALENCE BAND EDGE (eV)
E
1
0
-1
-2
-3
Au
a-Ge
hν=7.7 eV
W
E
L_{mj}
L_{sc}
$\frac{W}{2}$
32
VBE
E_f

Figure 4

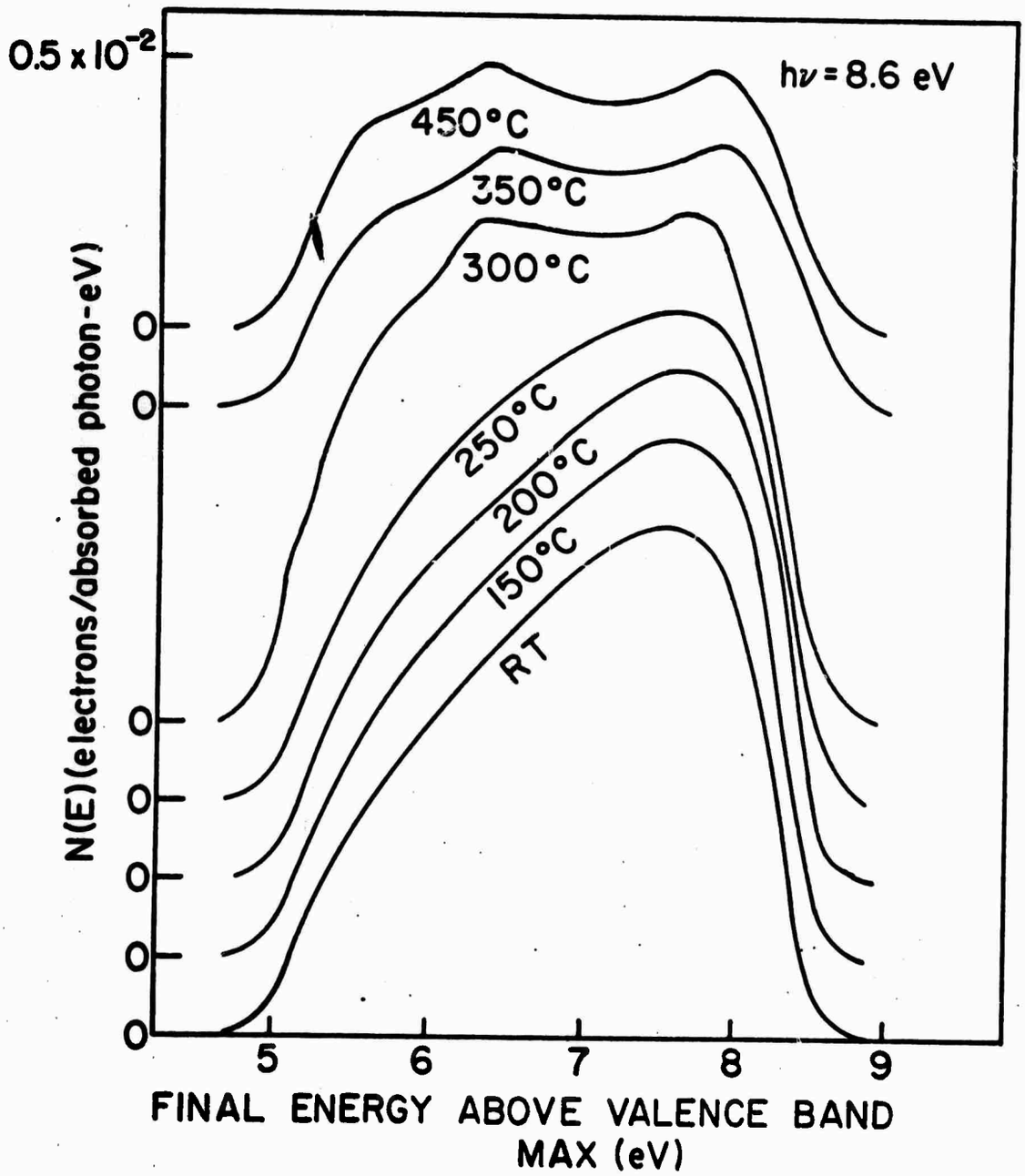
0.5 x 10⁻²
hν = 8.6 eV
450°C
350°C
300°C
250°C
200°C
150°C
RT
N(E) (electrons/absorbed photon-eV)
0
0
0
0
0
0
5
6
7
8
9
FINAL ENERGY ABOVE VALENCE BAND MAX (eV)

Figure 5

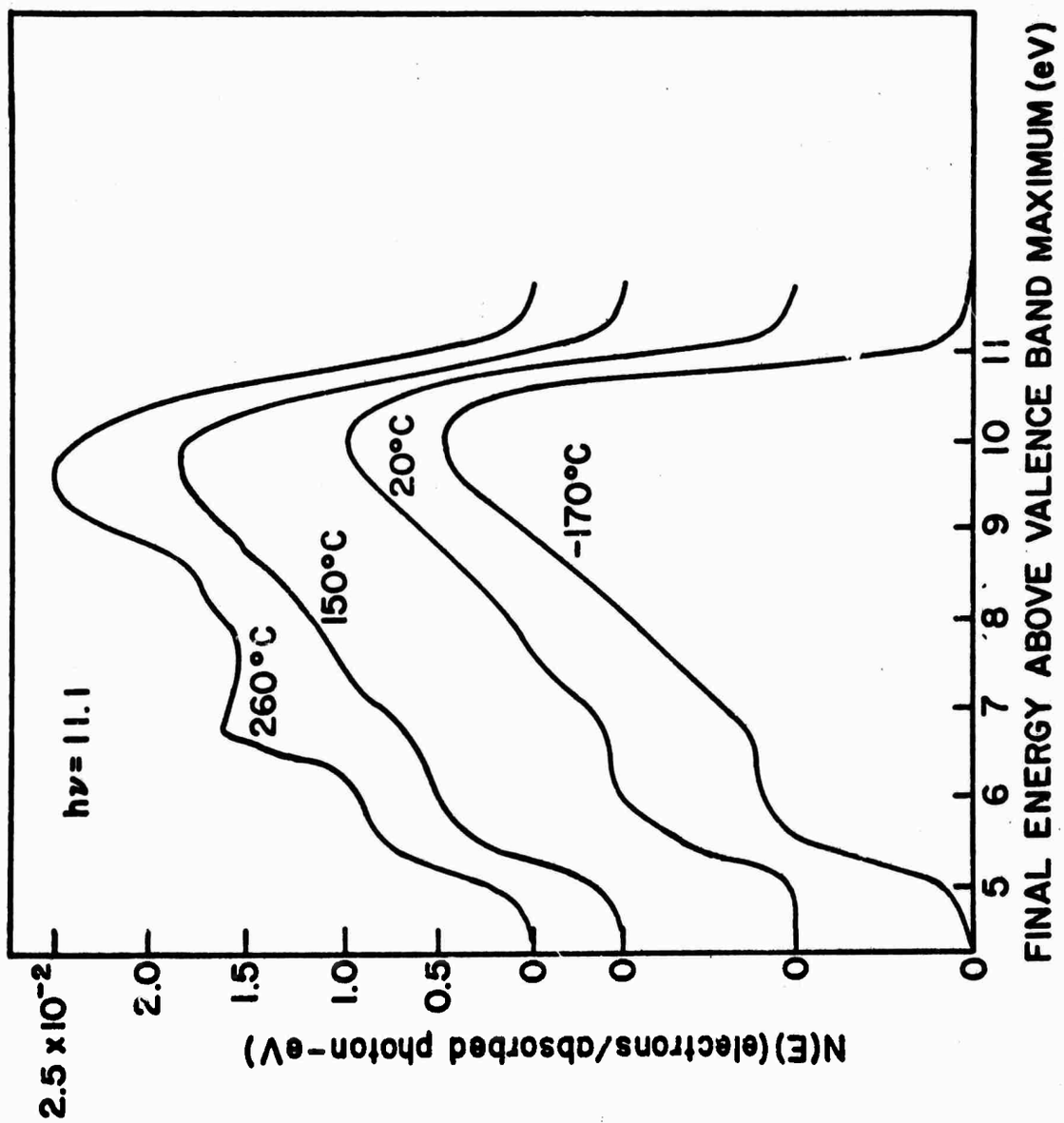
hν= 11.1
260°C
150°C
20°C
-170°C
N(E)(electrons/absorbed photon-eV)
2.5 x10⁻²
2.0
1.5
1.0
0.5
0
0
0
0
5
6
7
8
9
10
11
FINAL ENERGY ABOVE VALENCE BAND MAXIMUM (eV)

Figure 6

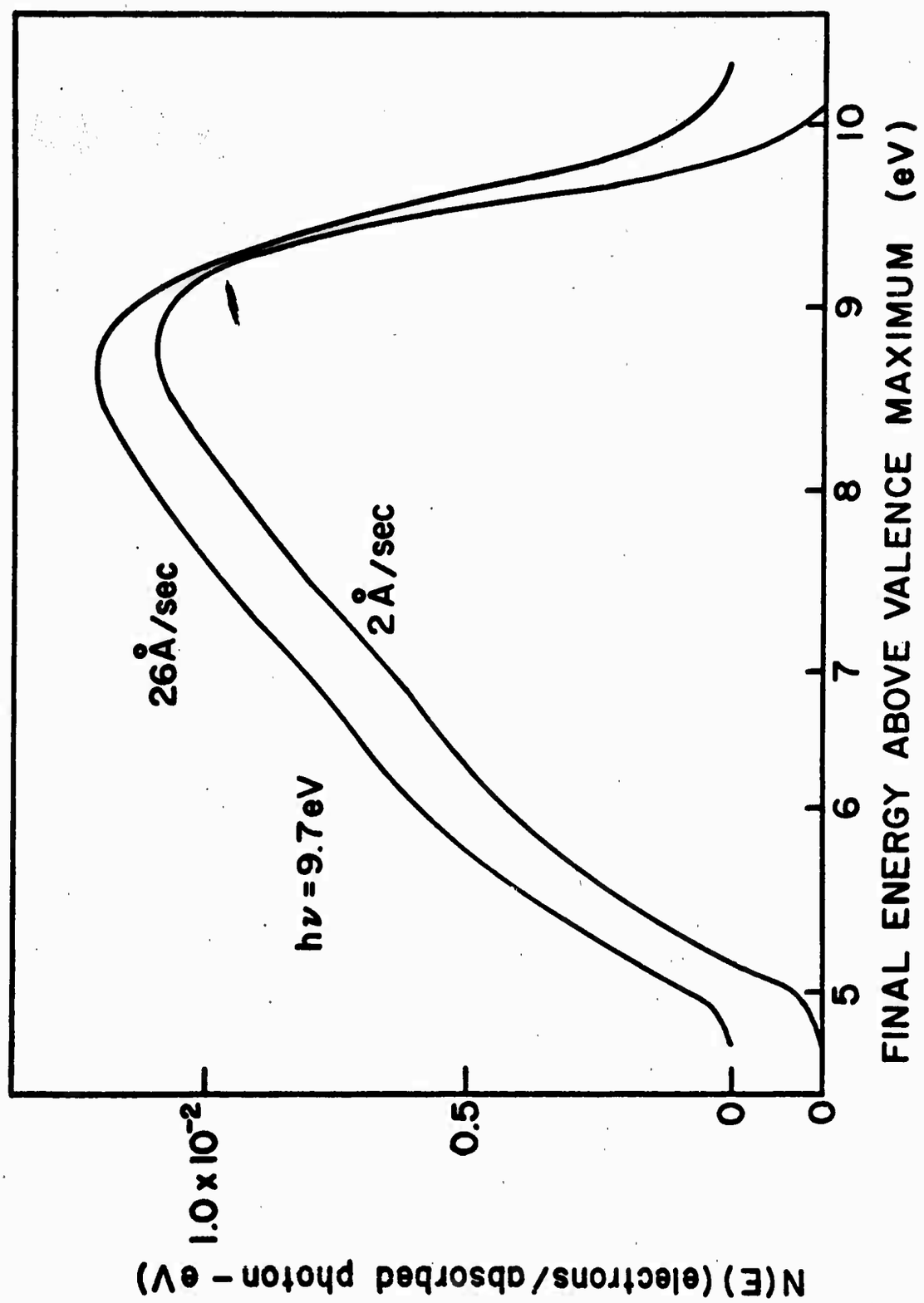
N(E) (electrons/absorbed photon – eV)
1.0 x 10⁻²
0.5
0
0
5
6
7
8
9
10
FINAL ENERGY ABOVE VALENCE MAXIMUM (eV)
hν=9.7eV
26Å/sec
2Å/sec

Figure 7

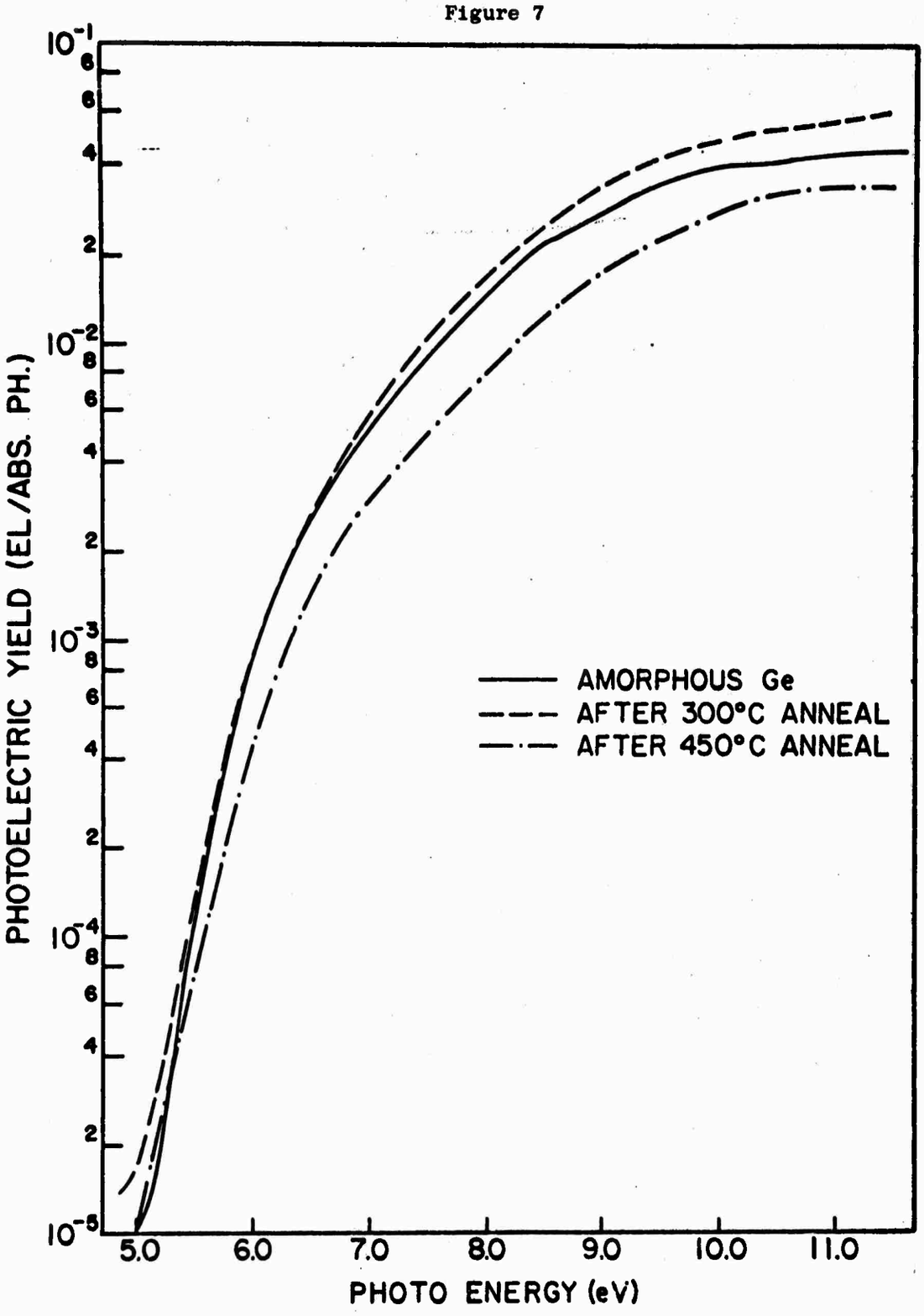
PHOTOELECTRIC YIELD (EL/ABS. PH.)
PHOTO ENERGY (eV)
AMORPHOUS Ge
AFTER 300°C ANNEAL
AFTER 450°C ANNEAL
5.0
6.0
7.0
8.0
9.0
10.0
11.0

Figure 8

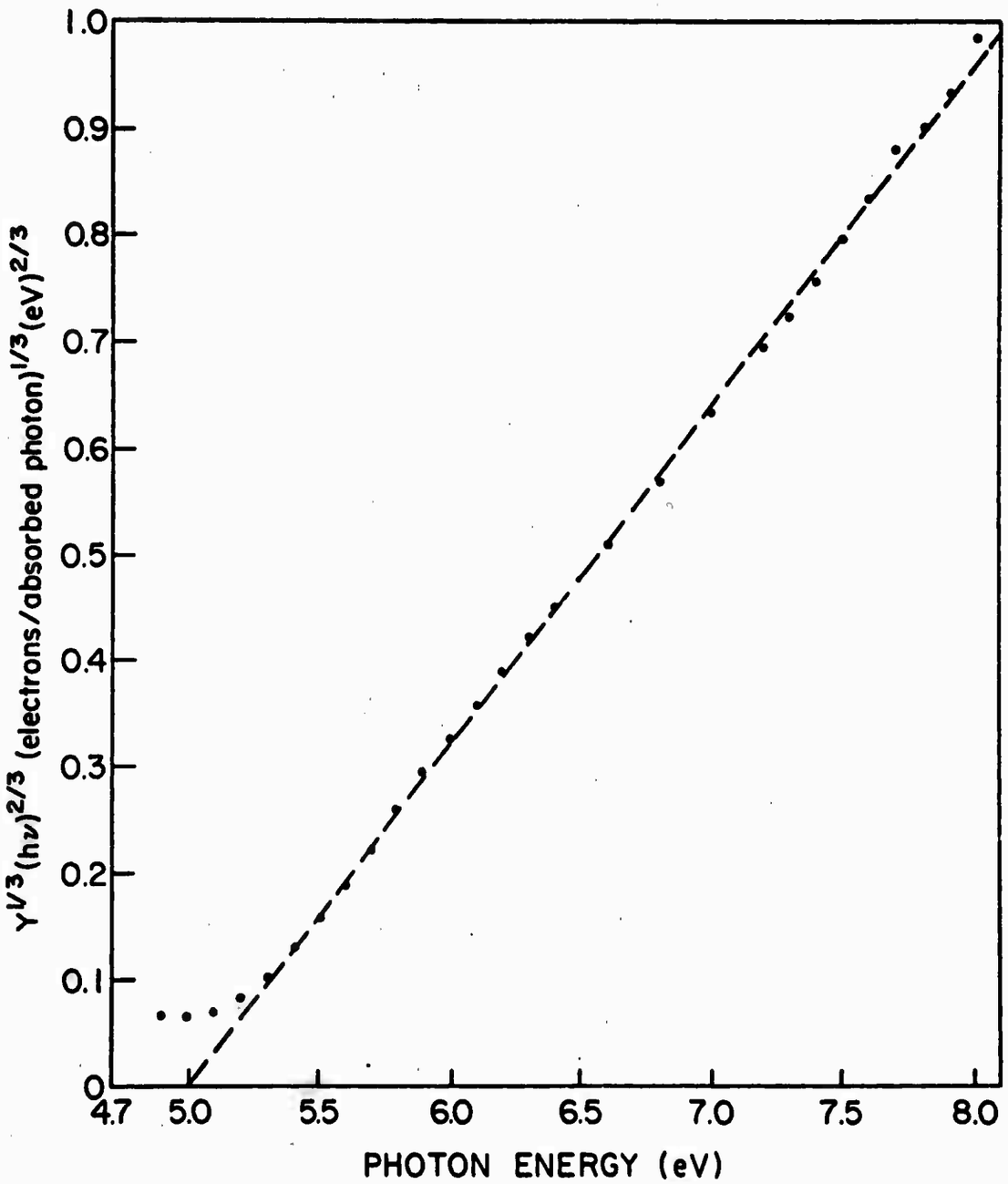
1.0
0.9
0.8
0.7
0.6
0.5
0.4
0.3
0.2
0.1
0
4.7
5.0
5.5
6.0
6.5
7.0
7.5
8.0
PHOTON ENERGY (eV)
Y^1/3(hν)^2/3 (electrons/absorbed photon)^1/3(eV)^2/3

C. Considerations of Results from Amorphous Ge and Si (W. E. Spicer)

1. Introduction

Some time during the past year has been spent in examining the data generated at Stanford on amorphous Ge, Si and related materials and in trying to understand the possible implications of these results. In this part of the report we will discuss two aspects of this study. The first is the density of states of the amorphous material, as obtained from the photoemission and optical measurements and its comparison with the density of states of the crystalline material. The second is Fermi level pinning by surface states and its possible effect on transport measurements. It should be emphasized that we are presenting tentative models for the purpose of stimulating discussion and future work.

2. Density of States--Chemical and Bragg Band Gaps

In Figure 9 and 10 we present the optical density of states of amorphous Ge as obtained by Donovan and Spicer.[1] As can be seen in Fig. 10, the band edges are found to be quite sharp. Further confirmation for these sharp edges has been found in the recent photoconductivity work of Fischer and Donovan.[2] Pierce and Spicer[3] and Fischer and Donovan[4] have also recently found evidence for a sharp absorption edge in Si. It thus appears that it is possible to form an amorphous solid while retaining band edges which are as sharp and well defined as those in the crystalline material. This is a very important result since it is strongly disagreeable with the starting assumptions inherent to the Mott-Cohen models for the electronic structure of amorphous solids. The potential practical implications are far reaching. Recent theoretical

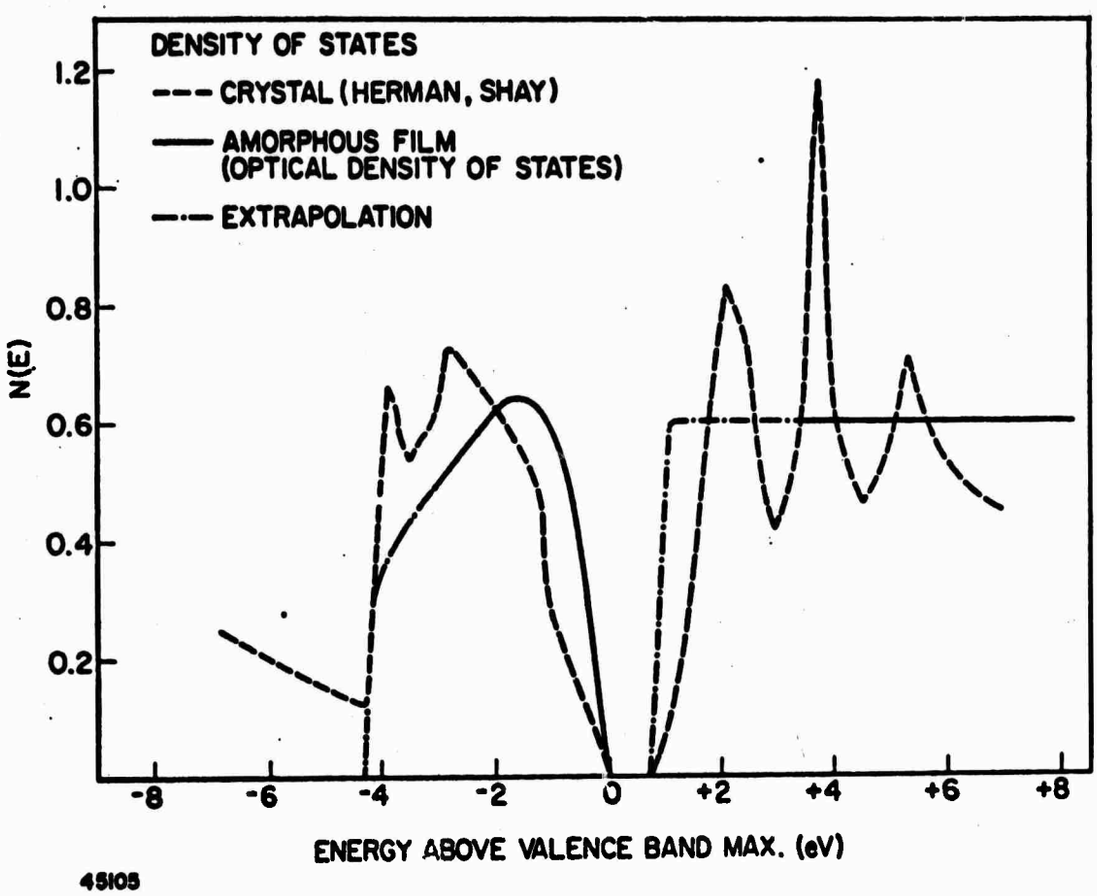

Figure 9. Optical Density of States for Amorphous Ge.

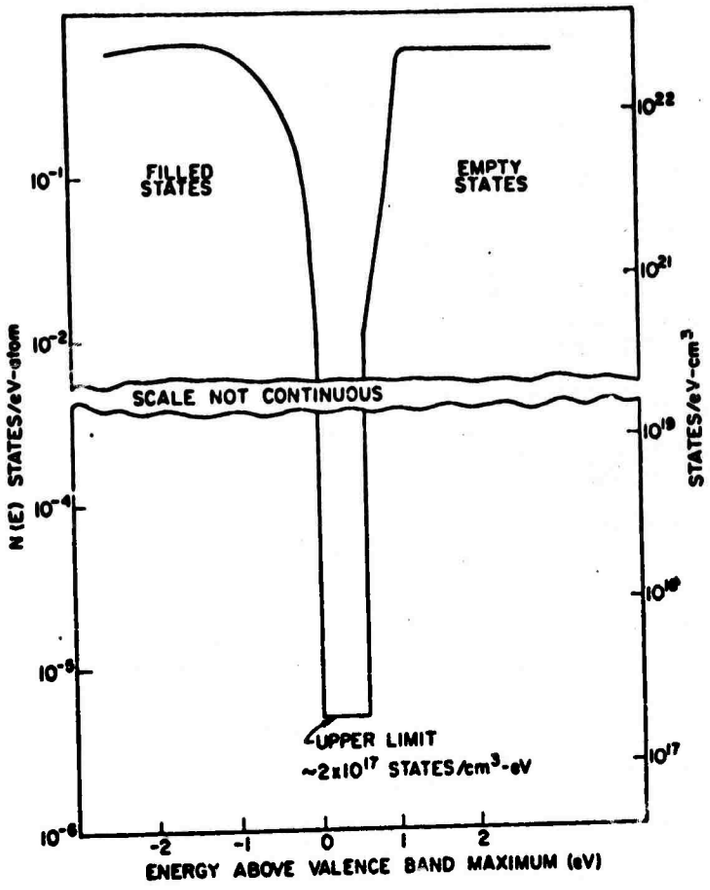

Fig. 10. Optical Density of States for Amorphous Ge.

work by Weaire[6] and Heine[7] has shown that theoretical models are possible for amorphous materials which do not require the loss of sharp band edges.

At first sight the retention of sharp band edges seems at odds with a striking feature of Fig. 9. This is the loss of the sharp structure in the crystalline density of states on going to the amorphous material. In the crystalline materials, there are sharp conduction band peaks at about 2.1, 3.9, and 5.5 eV. There are also peaks in the valence band at -2.6 and -3.9 eV. All of this structure disappears in the amorphous materials. Why does this structure disappear while the band edges remain sharp? In order to understand this, it seems useful to make a distinction between two types of band gaps: 1) chemical gaps which are primarily the result of the chemical character of the material, for example the covalent band in the present case, and 2) Bragg gaps which are related to long-range order and the Bragg reflection condition. As can be seen from an examination, the large peaks in the crystalline density of states are due principally to states near the zone face where the effects of Bragg reflection would be greatest. Thus it is not surprising that these peaks should disappear when long-range order and thus the Bragg reflection condition is eliminated.

In contrast, the sharp band edges of the forbidden gap remain in the amorphous material. This is attributed to the fact that the covalent bond is retained almost undisturbed in the amorphous material and the minimum band gap is closely related to the covalent bond. In recognition of its chemical nature, this band gap is called a chemical gap. The sharpness of the gap in the amorphous material is probably a reflection of how well the covalent bond is defined; however, the gap energy is, of course, much less than the covalent bond energy.

With these thoughts in mind, one can take a new look at the crystalline and amorphous density of states of Fig. 9. In the amorphous material the principal constraint on the density of states is the covalent bond; thus, the density of states for the amorphous material can be thought of as the density of states imposed principally by the covalent bond.

For the crystalline material, a second major constraint is added, that of long-range order; this produces Bragg reflection and band structure in the sense of the Bloch theorem with $\bar{k}$ being a good quantum number. As a result of this added set of constraints, the sharp peaks shown in Fig. 9 appear in the density of states of the crystalline material. Thus, it is suggested that the density of states of the amorphous material reflects principally the constraints set by the covalent bond; whereas, the density of states of the crystalline material results from the constraints set by long-range crystalline order as well as the covalent bond.

3. Micro-Voids, Fermi Level Pinning, and Other Thoughts

In recent years, evidence has grown that micro-voids, i.e., holes or pores about 10 Å across, can play an important role in amorphous Ge and Si. Ehrenreich and Turnbull[8] have made some tentative suggestions concerning this in terms of a "Swiss Cheese" model of amorphous Ge and Si. The micro-voids also may be important in more complex amorphous materials although this has not been established. Hence, we will expand on the previous considerations and make certain new suggestions. The variation of density in various amorphous Ge samples seems

to be due to the presence of micro-voids. However, the work of Donovan, Ashley and Spicer[9] indicates that by properly choosing the temperature of the substrate on which the amorphous material is formed, one can virtually eliminate the micro-voids and obtain a density quite similar to that of crystalline Ge. The message seems clear: if an evaporated Ge atom is to find an "ideal" site as the amorphous material is formed, it must have sufficient mobility and this mobility is thermally activated. If there is insufficient mobility, defects occur in the films. These defects coalesce in the form of micro-voids. Just as dislocations are the dominate form of imperfection in crystalline Ge, micro-voids appear to be dominant in amorphous Ge. It may be useful to think of micro-voids in amorphous Ge playing a role similar to that played by dislocations in crystalline Ge.

One striking thing about the annealing of amorphous Ge to form the crystalline material is the fact that the transition temperature can vary over several hundred degrees depending on conditions under which the material is formed. It has been found that the better the vacuum conditions, the lower the temperature at which the amorphous Ge crystallizes.[10] This suggests that any oxygen present in the film will tend to be on the surfaces of micro-voids stabilizing the micro-void. In crystalline materials, radiation damage studies have shown that vacancies formed by irradiation tend to be trapped by oxygen impurities in the lattice. In a similar manner, oxygen impurities probably prefer to be on the surfaces of voids rather than at random sites in the bulk of amorphous Ge. The oxygen also probably helps nucleate and stabilize micro-voids in the amorphous Ge. To carry forward the analogy between dislocations and micro-voids, oxygen impurities probably increase the micro-void

count in amorphous Ge just as they increased the dislocation count in crystalline Ge.

The energy of Ge containing oxygen impurities would certainly be reduced if the oxygen were transferred from the bulk to the surfaces of micro-voids since the oxygen on the surface of the micro-void could "bridge" between surface bonds which were formerly "dangling." Conversely, if the micro-voids are to be removed either to form more dense amorphous Ge and/or in the process of crystallizing the film, considerable additional energy must be supplied if oxygen impurities must be moved from positions where they bridge "dangling" bonds on micro-void surfaces to bridging sites in the bulk of the material. Thus, one would expect oxygen to stabilize the micro-voids and thus increase the amorphous-crystalline transformation temperature in agreement with practical experience.

The effect of micro-voids on the electronic properties of amorphous materials should not be overlooked. It is well established that surface states often associated with "dangling" bonds on the surfaces of crystalline Ge and Si pin the Fermi level at the surface. Usually, the position of the Fermi level at the surface is different from that in the bulk of the material resulting in band bending at the surface. One should expect similar pinning at the surfaces of the micro-voids. Since the micro-voids will be distributed throughout the bulk of the amorphous material, micro-functions and the undulation band structure suggested by Fritzsche,[11] Tauc,[12] and others could result. This could possibly give rise to many of the aspects of transport phenomena such as activated mobility which has previously been associated with mobility gap models. It should be noted that this undulation would not necessarily result from band tailing effects but simply from the presence of micro-voids.

It has been shown that one can obtain large spin resonance signals from amorphous Si.[13] These signals have the same character as those from the surfaces of crystalline samples. It seems reasonable to associate them with the surface states on the walls of micro-voids.[14] It seems important that experiments be done to see if the strength of the spin signal correlates inversely with the density of the amorphous sample as would be expected if it were due to micro-voids. It has been observed that the spin signal goes down as the sample is annealed in agreement with a micro-void model.[13]

There have been attempts to correlate the spin signal with optical absorption.[15] Care should be taken in doing this. Since the wave functions associated with the surface states are spacially separated from the conduction and valence band states, the matrix elements coupling surface states with band states may be very weak. Only if strong excitation is possible for $h\nu < E_g$ will the surface states give rise to measurable absorption. If the energy separation between the ground state and excited surface states to which they strongly couple is larger than the band gap, it will be very difficult to detect the surface states by optical means. Thus one should not necessarily expect correlation between the resonance signal and optical absorption lying below the band gap.

Attempts have been made to use capacitance measurements to determine the density of states in the forbidden gap of amorphous semiconductors. If micro-voids were present, the surface states could dominate the experiment and thus the density of micro-void surface states might be confused with a density of bulk states in the forbidden gap. Likewise,

the micro-void surface states might provide trap states in photoconductive and transport measurements.

As mentioned earlier, according to the Mott-Cohen model, when long-range order is destroyed, as in an amorphous material, the sharpness of the band edges is also destroyed, leading to abnormal tailing of states into the gap. Recent optical absorption, photoconductivity, and photoemission studies of amorphous Ge and Si have failed to give evidence for any such tailing. Rather, the band edge seems to be as sharp in the amorphous as in the crystalline forms of these materials. More recently, theoretical results have been obtained which argue against the necessity for the loss of a sharp edge in amorphous Ge and Si.[6,7] It appears important to reexamine the experimental evidence for band tailing from magnetic and transport measurements to see if it really requires the necessity for the assumption of a greater number of states in the gap than are found in comparable crystalline materials. In this reexamination, it is important to see if phenomena previously ascribed to band tailing in the bulk may indeed be due to the effects of micro-voids mentioned above.

1. T. M. Donovan and W. E. Spicer, Phys. Rev. Letters 21, 1572 (1968); 22, 1058 (1969); W. E. Spicer and T. M. Donovan, J. Non-Cryst. Solids 2, 66 (1970); T. M. Donovan, W. E. Spicer, J. M. Bennett and E. J. Ashley, Phys. Rev. B2, 397 (1970); W. E. Spicer, T. M. Donovan and E. J. Ashley, Phys. Letters 32A, 85 (1970).

2. J. E. Fisher and T. M. Donovan, Optics Comm. 3, 116 (1971).

3. D. A. Pierce and W. E. Spicer, to be published.

4. J. E. Fisher and T. M. Donovan, to be published.

5. M. H. Cohen, Phys. Today 24, 26 (1971).

6. D. Weaire and M. F. Thorpe, to be published.

7. V. Heine, private communication.

8. H. Ehrenreich and D. Turnbull, Comments on Solid State Phys. 3, 75 (1970).

9. T. M. Donovan, E. J. Ashley and W. E. Spicer, Phys. Letters 32A, 85 (1970).

10. R. F. Adamsky, J. Appl. Phys. 40, 4301 (1969).

11. H. Fritzsche, J. Non-Cryst. Solids, in press.

12. J. Tauc, private communication.

13. M. H. Brodsky, R. S. Title, K. Weiser and G. D. Pettit, Phys. Rev. B1, 2632 (1970).

14. S. C. Moss and J. F. Grazcyk, Phys. Rev. Letters 23, 1167 (1969).

15. J. Tauc, A. Menth and D. Wood, Phys. Rev. Letters 25, 749 (1970).

BLANK PAGE

II. BINARY MATERIALS

This section presents studies on binary amorphous materials. The initial subsection describes recent efforts to build up sputtering capabilities for these and more complex materials. The following subsections deal with x-ray diffraction, neutron diffraction, electron microscopy, x-ray photoemission, x-ray absorption edge and ultraviolet photoemission studies designed to elucidate the atomic arrangements, bonding types and electronic densities of states in amorphous and crystalline materials in the Ge-Te system. Then, experimental preparations for ultraviolet photoemission studies of As_2Se_3 and Se are briefly discussed. Finally, initial structural studies in the Si-Te system are discussed.

Preceding page blank

A. Thin-Film Sputtering Capabilities (Y. Verhelle and T. Arnoldussen)

In a number of studies which are to be performed during the coming year, thin films of binary and more complex amorphous alloys must be prepared in special geometries which include thin film electrodes. Such samples have, in the past, been provided for us by Energy Conversion Devices, Inc. As our program increased in magnitude, and with the increasing coordination between different groups here, it became important to be able to prepare many samples of the same composition for different types of investigations (phase separation, electrical transport, etc.). As a result, considerable effort has been put into the acquisition of skills necessary for the production of high quality sputtered films. During the course of this work, we have studied various methods of cathode preparation and the dependence of cathode quality (grain size, composition homogeneity, packing coefficient and cathode lamination) as a function of pressing conditions for samples in the Ge-Te system. Thus far, three high quality cathodes in this system have been prepared. This work was performed on borrowed equipment so that we might purchase our own equipment intelligently. With the experience gained, we have ordered the ball mill, hot press and glove box which should be appropriate for our needs. With the arrival of this equipment, we expect to be able to prepare cathodes as needed.

At the same time, we have been developing sputtering skills with the prepared cathodes and have produced fairly high quality thin films for phase separation and photocrystallization studies.

B. X-Ray and Neutron Diffraction Radial Distribution Studies of Amorphous Ge-Te Alloys (F. Betts, A. Bienenstock and D. Keating)

In earlier work[1,2] we examined the structures of amorphous GeTe and various Ge_xTe_{1-x} alloy films by means of x-ray diffraction radial distributions. The most important result of these studies was that the interatomic distances throughout the compoisition range studied ($.1< x <.7$) appeared covalent. This result is consistent with the Mott[3] or Cohen, Fritzsche and Ovshinsky[4] pictures of why many amorphous semiconductor conductivities are so insensitive to many impurities. In these pictures, each atom is coordinated such that covalent bonding requirements are satisfied locally. As a result, no significant number of donor or acceptor states are formed. The result is particularly striking because the crystalline GeTe, which would appear throughout the composition range studied, in equilibrium, has significantly larger nearest neighbor GeTe separations which cannot be described in terms of simple covalent bonding.

For the alloys which are dilute in Ge, it was proposed by us[2] that the structure is one in which Ge atoms cross-link Te chains. The best evidence for this structure came from careful analysis of an x-ray diffraction radial distribution obtained from a film of composition $Ge_{.11}Te_{.89}$.

This x-ray diffraction study was inconclusive for a number of reasons. The first is that any such x-ray radial distribution study is necessarily ambiguous, as discussed by Keating.[5] More important, however, is the fact that it was difficult to make strong statements about the Ge coordination because the Ge concentration in the alloy is low and because the Ge x-ray scattering factor is significantly smaller than that of Te. As a result, Ge bonding contributions to the area of the first radial distribution peak were small.

In an effort to attach greater certainty to the above-mentioned bonding picture, we have performed[6] both x-ray and neutron diffraction radial distribution studies of amorphous $Ge_{.17}Te_{.83}$. Of these, the neutron diffraction study is most important and is discussed here extensively. Neutron diffraction offers a number of significant advantages for such studies in this system. First, the scattering factors of the two species are independent of scattering angle. As a result, certain approximations which must be made in the analysis of x-ray diffraction data need not be made in the neutron case. Second, since the scattering is truly nuclear, and because the above-mentioned approximations are not necessary, significantly higher resolution can be obtained in the final radial distribution. Third, and extremely important, is the fact that the neutron scattering factor of Ge is approximately 50% larger than that of Te. As a result, the radial distribution obtained is significantly more sensitive to Ge coordination than is the corresponding x-ray diffraction radial distribution on the same sample. These virtues have shown themselves to be extremely important, as is indicated below.

The most striking disadvantage of neutron diffraction for studies of many amorphous semiconductors is that fairly large quantities of bulk material are required, whereas most of these samples can only be prepared through vapor deposition. Fortunately, Dr. J. deNeufville of Energy Conversion Devices, Inc. developed a technique for preparing bulk samples of $Ge_{.17}Te_{.83}$ and made them available for this study.

The neutron diffraction radial distribution is shown in Fig. 11. The most striking features of this distribution, indicating its high quality, are the absence of structure for R less than 2 Å, and the

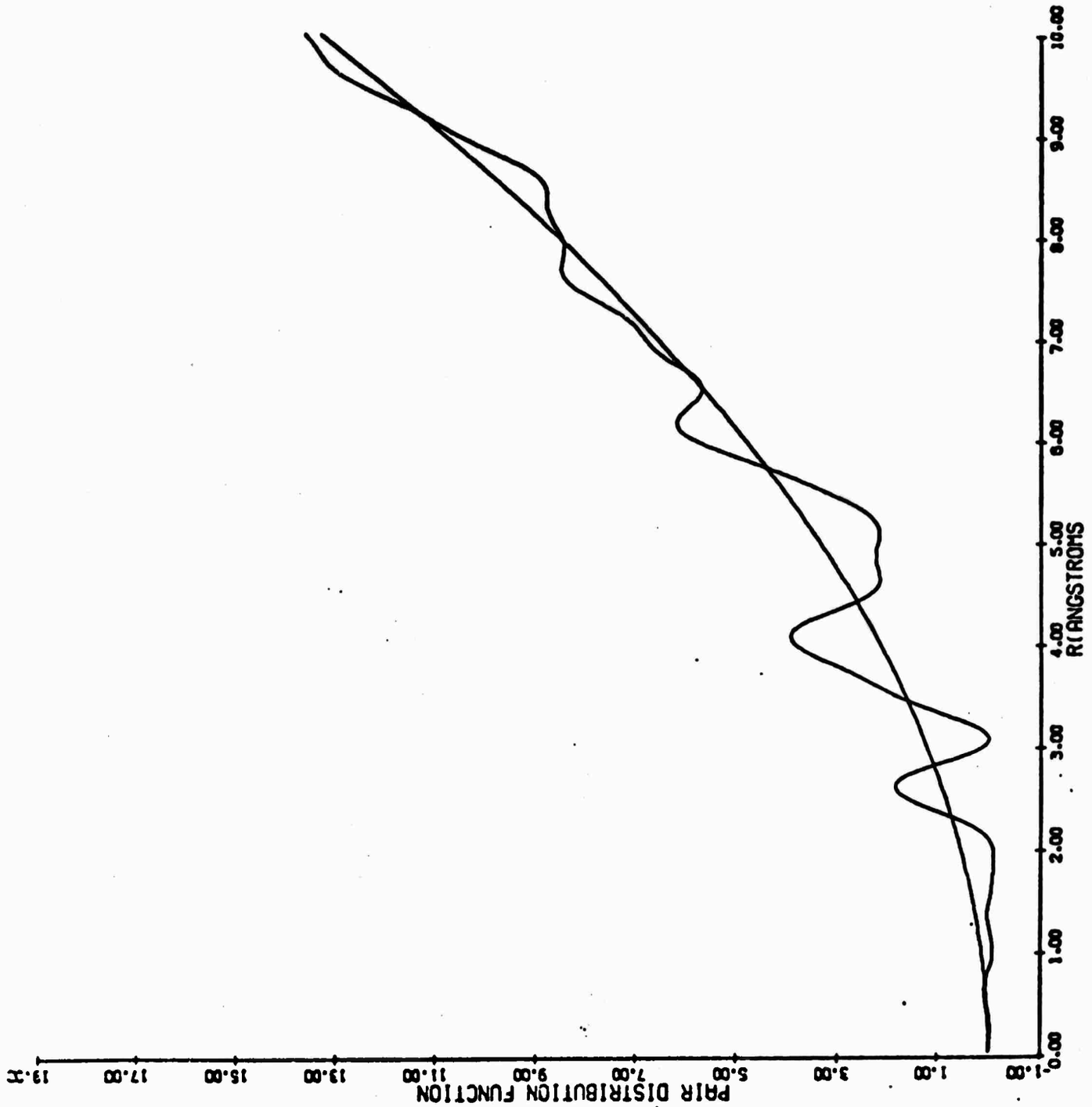

Figure 11. Neutron Diffraction Radial Distribution Function for $Ge_{17}Te_{83}$.

almost perfect resolution of the first neighbor peak. The absence of structure indicates that there are no serious errors in the intensity data, or its analysis. This, coupled with the high resolution, has allowed us to obtain an extremely accurate area.

Our analysis of the radial distribution leads to the following conclusions.

1. The area of the first neighbor peak agrees to 1 part in 900 with the area calculated from the "Random Covalent Model" of Betts et al[2] and to approximately 2% with the area calculated from their "Dilute x Model". Hence, these areas lend strong support for the validities of the models. Each of these models have as their basis the four-fold coordination of Ge and two-fold coordination of Te, in keeping with the structural picture of Mott-Cohen, Fritzsche and Ovshinsky. They differ only in the details of the arrangement.

2. The first peak of the radial distribution is at 2.65 Å. This is only slightly longer than the expected covalent GeTe separation of 2.57 Å. This slight discrepancy is to be expected, since Te-Te bonds still account for approximately 40% of the area. Note, however, that this distance is significantly smaller than the 2.84 Å nearest neighbor Ge-Te separation in crystalline GeTe, where the bonding is almost semi-metallic in nature.

Hence, we believe the results point strongly towards a picture of covalent bonding. Other experiments described below reinforce this conclusion.

In our previous descriptions of this work, we have also discussed the potential ambiguities in interpretation associated with the possibility of phase separation. Careful studies by Chaudhari,[7] as well as

our own initial efforts described below, indicate that there is no phase separation at the closely related composition $Ge_{.15}Te_{.85}$. Hence, this ambiguity has been removed.

Finally, we should indicate that we have considerably improved our x-ray diffraction procedures. As a result, we have just obtained better radial distributions from samples of different compositions. These will be analyzed and discussed in the next report.

1. A. Bienenstock, F. Betts, and S. R. Ovshinsky, J. Non-Crystl. Solids 2, 347 (1970).

2. F. Betts, A. Bienenstock and S. R. Ovshinsky, J. Non-Crystl. Sclids 4, 554 (1970).

3. N. F. Mott, Advan. Phys. 16, 49 (1967).

4. M. H. Cohen, H. Fritzsche and S. R. Ovshinsky, Phys. Rev. Letters 22, 1065 (1969).

5. D. T. Keating, J. Appl. Phys. 34, 923 (1963).

6. A. I. Bienenstock, F. Betts, D. T. Keating and J. deNeufville, Bull. Amer. Phys. Soc. 15, 1616 (1970). A manuscript is now being prepared for publication. This work was partially supported by the Atomic Energy Commission through Brookhaven National Laboratory's neutron diffraction facilities and Dr. Keating's participation. In addition, Dr. deNeufville's participation was supported by Energy Conversion Devices, Inc.

7. P. Chaudhari, private communication.

C. Phase Separation in Ge-Te Films (Y. Verhelle, G. Fisher and A. Bienenstock)

As indicated above, one source of ambiguity in the radial distribution studies performed by us on the Ge-Te alloy system is associated with the possibility that the materials phase separate. Hence, we have searched for phase separation in sputtered Ge_xTe_{1-x} films with compositions, $x = 0.2$, 0.33 and 0.5, as well as evaporated films with $x = 0.5$, using transmission electron microscopy. In all cases, the films were deposited onto carbon coated electron microscope grids. The evaporated films are of the type used for ultraviolet photoemission studies.

Thus far, no phase separation has been observed. We have thought of three possible explanations for this. The first is that the systems do not "want" to phase separate. Some evidence supporting this picture comes from two sources. The first is the glass transition temperature versus composition study on the Ge-Te system by J. deNeufville.[1] He finds no evidence of the plateau expected when there is phase separation. In addition, P. Chaudhari[2] has studied samples of the composition $x = 0.15$. He finds no separation in these materials even when they are maintained at elevated temperatures. Indeed, the materials seem to crystallize without any tendency for liquid-liquid separation. This second observation cannot, however, be used to rule out separation for compositions other than $x = 0.15$.

It is also possible, however, that the samples studied never reached sufficiently elevated temperatures so that there was sufficient mobility for phase separation. For this reason, we have obtained a hot stage for the electron microscope and are reexamining the films at elevated temperatures.

Finally, it is possible that we have missed the phase separation through inexperience in observing it. To make sure that this is not the case, and to obtain experience, we are now preparing films of materials which are known to separate.

1. J. deNeufville, private communication.

2. P. Chaudhari, private communication.

D. X-Ray Induced Photoemission Studies (F. Betts, A. Bienenstock and C. Bates)

In the original research proposal for this contract, it was indicated that we intended to examine the feasibility of using x-ray induced photoemission and x-ray absorption edge measurements for the study of bonding and coordination of impurities in amorphous materials. Results obtained thus far indicate that these are, indeed, most valuable tools.

In our earlier radial distribution work, it was shown that the Ge-Te amorphous alloys can be characterized by covalent bond distances. The existence of the covalent bonding is obtained by inference. The results obtained with the x-ray photoemission and absorption edge techniques are much more direct in their indication of covalent bonding. Both work on essentially the same principle. Since the photoemission is somewhat better understood, it is described first.

When an atom loses an electron through, say, the classical type of ionic bonding, its core electrons are more strongly bound to the nucleus. As a result, the energy required to create a free core electron of fixed kinetic energy through the x-ray photoemission effect, is greater. By measuring the kinetic energies of electrons ejected through irradiation by characteristic x-rays, it is possible to measure the bonding energies relative to the Fermi energy of the sample in contact with the spectrometer.

In the work described here, performed on a Varian IEE spectrometer, we have studied both Ge and chalcogenide core shell binding energies in various Ge-chalcogen alloys and compounds. The work shows, quite definitively, that the core shell binding energies are significantly greater in crystalline GeTe, GeSe and GeS than they are in the amorphous materials,

so that the bonding in the amorphous materials is significantly more covalent.

In Table 1, the measured shifts of the Ge $3d^{5/2}$ and appropriate chalcogen (Te $3d^{5/2}$, Se $3d^{5/2}$ or S $2p^{3/2}$) core levels are tabulated for a number of materials. The sign convention is chosen such that a positive shift indicates stronger binding and implies, for Ge, stronger ionicity. Similarly, the more negative the chalcogen shift, the more ionic it is.

Table 1. X-RAY PHOTOEMISSION SPECTROSCOPY DETERMINED BINDING ENERGY SHIFTS OF THE $Ge^{5/2}$ CORE LEVEL AND APPROPRIATE CHALCOGEN CORE LEVELS RELATIVE TO CRYSTALLINE Ge AND THE APPROPRIATE CHALCOGENS.

Sample	Ge Shift (eV)	Chalcogen Shift (eV)
GeTe (crystalline)	3.6	
GeSe (crystalline)	2.9	-2.7 (Se $3d^{5/2}$)
$Ge_{.15}Te_{.81}Sb_{.02}S_{.02}$ (amorphous)	1.1	
$Ge_{.15}Te_{.81}As_{.02}S_{.02}$ (amorphous)	1.1	+0.4 (Te $3d^{5/2}$)
$Ge_{.15}Te_{.81}As_{.02}S_{.02}$ (crystallized)	3.1	
$Ge_{.20}Te_{.80}$ (amorphous)	1.1*	+0.4
$Ge_{.33}Te_{.67}$ (amorphous)	1.0*	+0.4
$Ge_{.50}Te_{.50}$ (amorphous)	0.8*	+0.4
$Ge_{.57}Te_{.43}$ (amorphous)	1.1*	
GeS (crystalline)	1.9	-2.5 (S $2p^{3/2}$)

The shifts may be summarized in the following manner. In the crystalline materials, the Ge shift ranges from 1.9 to 3.6 eV, while in the amorphous materials it is approximately 1 eV. Similarly, the crystalline chalcogen shifts are of the order of -2.5 eV, while the amorphous shifts

are all +0.4 eV. The very large shifts for the crystalline materials and the very small shifts for the amorphous materials imply that the bonding in the amorphous materials is much more covalent than in the crystalline.

More detailed analyses of these shifts are now under way. Focus has centered about crystalline and amorphous GeTe. Here, work functions determined from work described in Section II.F of this report are available. For the crystalline GeTe, in accord with the work of Fadley, et al,[1] we have attempted to account for the Ge shift in terms of two predominant contributions. These are the free ion core shifts, as a function of ionization, as obtained from Hartree-Fock calculations,[2] and the Madelung field contributions. Unfortunately, the shift calculated from these two effects is too small, relative to the measured value, unless an extremely large effective charge is chosen. Efforts to resolve this difficulty are now in progress. It should be pointed out, however, that other workers[1] with this method have faced similar difficulties.

1. C. S. Fadley, S. B. M. Hagstrom, M. P. Klein and D. A. Shirley, J. Chem. Phys. 48, 3779 (1968).

2. E. Clementi, "Tables of Atomic Functions," a supplement to the paper, IBM J. Res. Dev. 9, 2 (1965).

E. X-Ray Absorption Edge Spectroscopy

Because the equipment is readily available at Stanford and could be improved for the performance of high accuracy work, we have also examined the bonding in amorphous Ge-Te alloys with x-ray absorption edge spectroscopy (XAES). While no satisfactory theory exists for the structure of the x-ray absorption edge, there is a considerable body of experimental data on a wide range of materials, including amorphous forms. A number of germanium compounds of particular interest have been investigated, including amorphous germanium, as well as the tetrahedral and octahedral allotropes of GeO_2.

Work here has been concerned, primarily, with measurements of the absorption edge energy in these materials. It has been found empirically that cation core level absorption edges shift to lower energies with increasing ionicity. Here, a decrease in energy is defined as a decrease in the photon energy associated with the absorption edge. As shown in Table 2, the amorphous Ge-Te alloys show Ge K_α absorption edge shifts of approximately -1.1 eV relative to crystalline Ge, while crystalline GeTe and GeSe show shifts of approximately -2.4 eV. These results should be compared with those for $GeSe_2$[1] and the two allotropes of GeO_2.[2] Covalently bonded, tetrahedrally coordinated Ge in $GeSe_2$ and the quartz structure of GeO_2 shows no measureable shift. In the ionic, rutile structure (octahedral coordination) form, the core shift is -6 eV. Hence, these results also indicate that the bonding in amorphous Ge-Te alloys, including amorphous GeTe, is considerably more covalent than in crystalline GeTe. The results also indicate our capability to determine covalent character with this technique. Further efforts are under way to increase the resolution of our equipment.

Table 2. SHIFTS OF THE Ge K_α ABSORPTION EDGE RELATIVE TO CRYSTALLINE Ge.

Sample	Shift (eV)
GeTe	-2.48 ± 0.1
GeSe	-2.35 ± 0.1
*$Ge_{.34}Te_{.66}$ (amorphous)	-1.16 ± 0.1
*$Ge_{.38}Te_{.62}$ (amorphous)	-1.13 ± 0.1
*$Ge_{.57}Te_{.43}$ (amorphous)	-1.11 ± 0.1
*$Ge_{.15}Te_{.81}Sb_{.02}S_{.02}$ (amorphous)	-1.31 ± 0.2
Ge (amorphous)	+1.0 ± 1.0
GeO_2 (quartz structure)	0.0 ± 1.0
GeO_2 (rutile structure)	-6.0 ± 1.0
$GeSe_2$	0.0 ± 0.4

1. C. Mande, R. Patil and A. Nigavekar, Nature 211, 518 (1966). C. Mande and R. Patil, Indian J. Pure and Appl. Phys. 3, 484 (1965).

2. E. W. White and H. A. McKinstry, in Advances in X-Ray Analysis, Vol. 9 (Plenum Press, New York, 1965).

F. Photoemission Studies of GeTe (G. B. Fisher and W. E. Spicer)

The photoemission study of germanium telluride is proceeding smoothly. The results obtained for amorphous GeTe are intriguing in themselves, but are also interesting because they are so different from the results for polycrystalline GeTe. Two of our aims are to gain knowledge of the density of states in the amorphous material and obtain an upper limit on the density of bulk states existing within the forbidden gap.

Electron energy distributions (EDCs) at photon energies from 6.2 eV to 11.7 eV and measurements of photoelectric yield have been obtained from amorphous and polycrystalline films sublimed from a source of polycrystalline GeTe. The amorphous films are evaporated onto a room temperature substrate (M_O), while the polycrystalline films were obtained both by annealing an amorphous film at 160°C and by evaporating onto a substrate held at 170°C. A quartz oscillator thickness monitor measured the thickness of films. Thicknesses between 1300 Å and 2500 Å were used. The pressure during evaporation reached 10^{-7} Torr in a system with a base pressure of 2×10^{-11} Torr. In order to attempt to look at states below the normal threshold, EDCs were taken on an amorphous film exposed to cesium.

The unnormalized EDCs in Fig. 12 show the results at three photon energies for an amorphous film. There are two relatively sharp peaks, 1.5 eV and about 3.1 eV below the high energy cutoff. All of the structure in the EDCs moves out in energy as $h\nu$ is increased according to the equation

$$E = h\nu + E_i ,$$

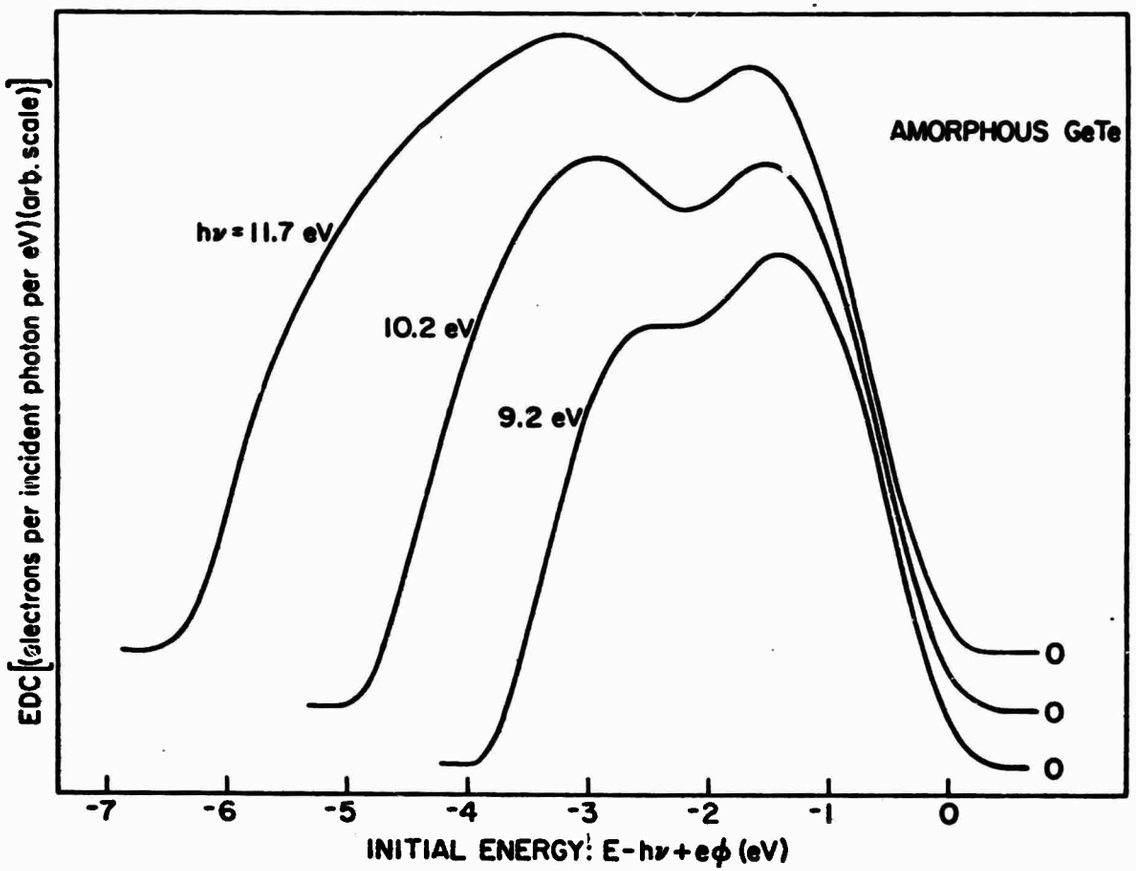

Fig. 12. Unnormalized EDCs from an Amorphous Film of GeTe.

where E is the final and E_i the initial energy. It is important to note that the shape of the structure does not change as it moves out. These facts together mean it is possible that the structure seen is representative of the density of filled states below the forbidden gap. The high energy cutoff is sharp. Further work should indicate to what degree states in the gap and/or instrumental broadening contribute to the leading edge.

The photoelectric yield of amorphous GeTe (Fig. 13) rises smoothly from threshold, leveling off at a yield of 0.015 electrons/incident photon at high energies. The yield of the polycrystalline films was nearly identical above threshold to the amorphous ones. However, the threshold as determined from the yield measurement is 5.02 ± .07 eV compared to 5.39 ± .07 eV for the amorphous material. The yield curves were best fit by the expression

$$Y = \frac{(h\nu - E_T)^3}{(h\nu)^2}$$

which gave each threshold energy (E_T).[1]

The EDCs of the polycrystalline film are strikingly different (Fig. 14) from those of amorphous GeTe. We no longer see two peaks moving with photon energy. The polycrystalline EDCs (Fig. 15) exhibit a shoulder about 0.9 eV back from the leading edge which moves directly with photon energy. However, the main peak moves away from the leading edge with increasing photon energy, indicating possible matrix element effects due to $\bar{k}$ conservation in transitions to that energy. The great difference in short range order between amorphous and polycrystalline GeTe[2,3]

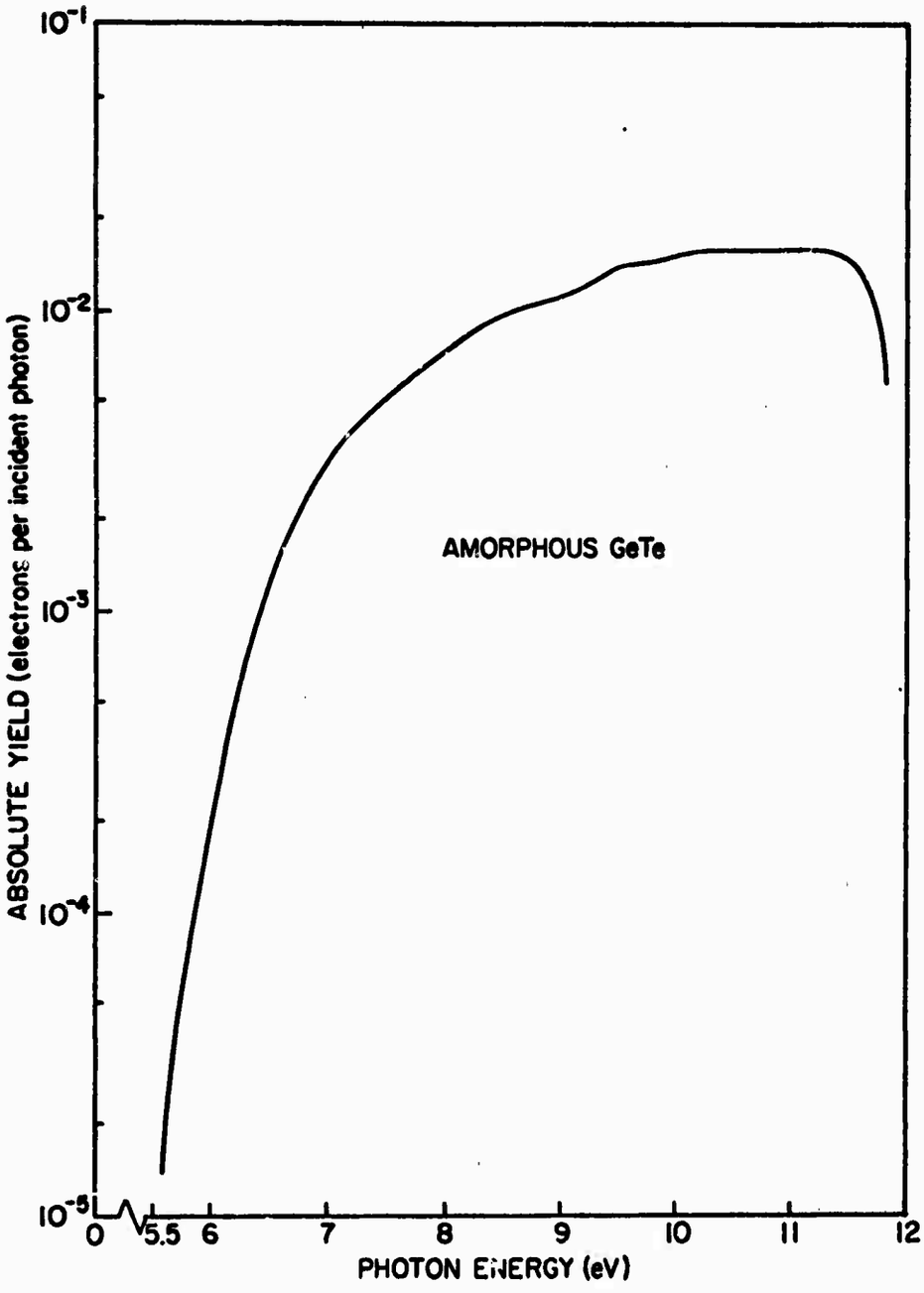

Fig. 13. Photoelectric Yield of an Amorphous Film of GeTe.

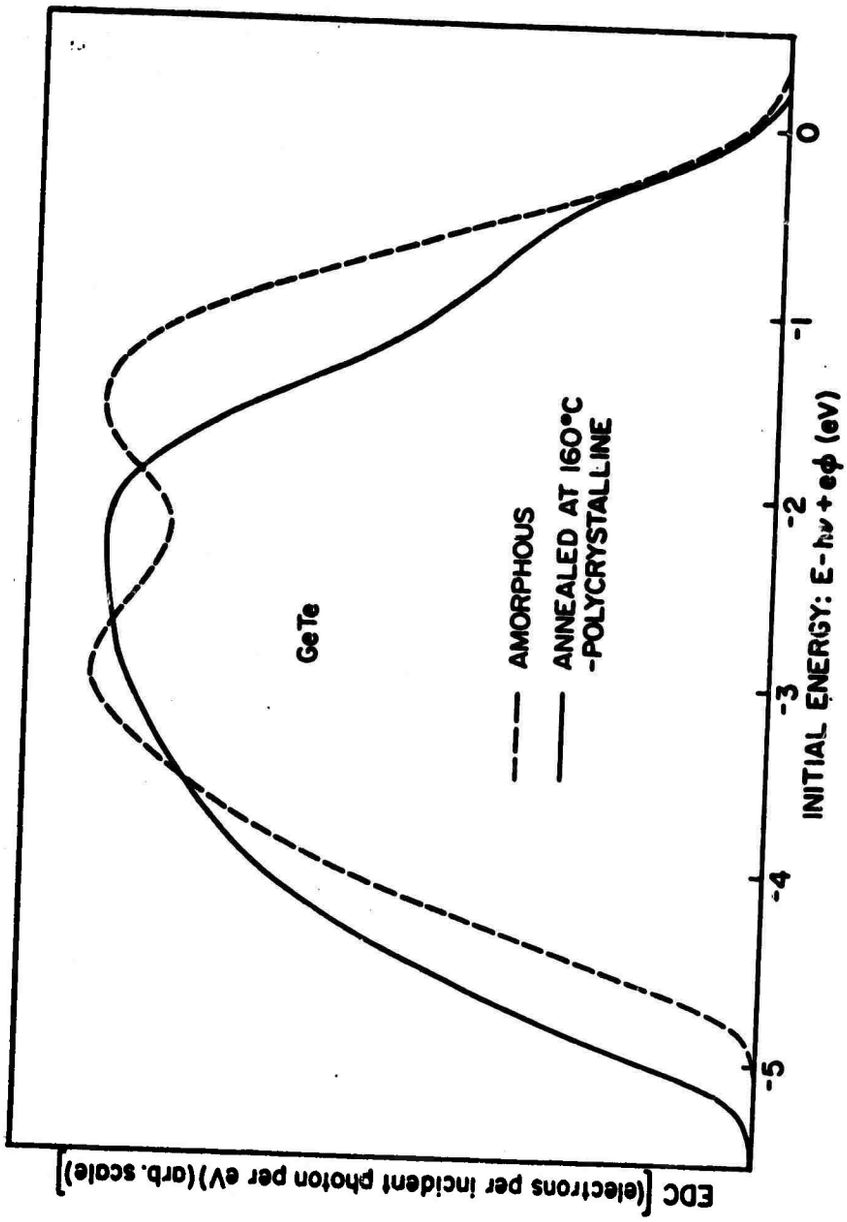

Fig. 14. Unnormalized EDCs from a GeTe Film.

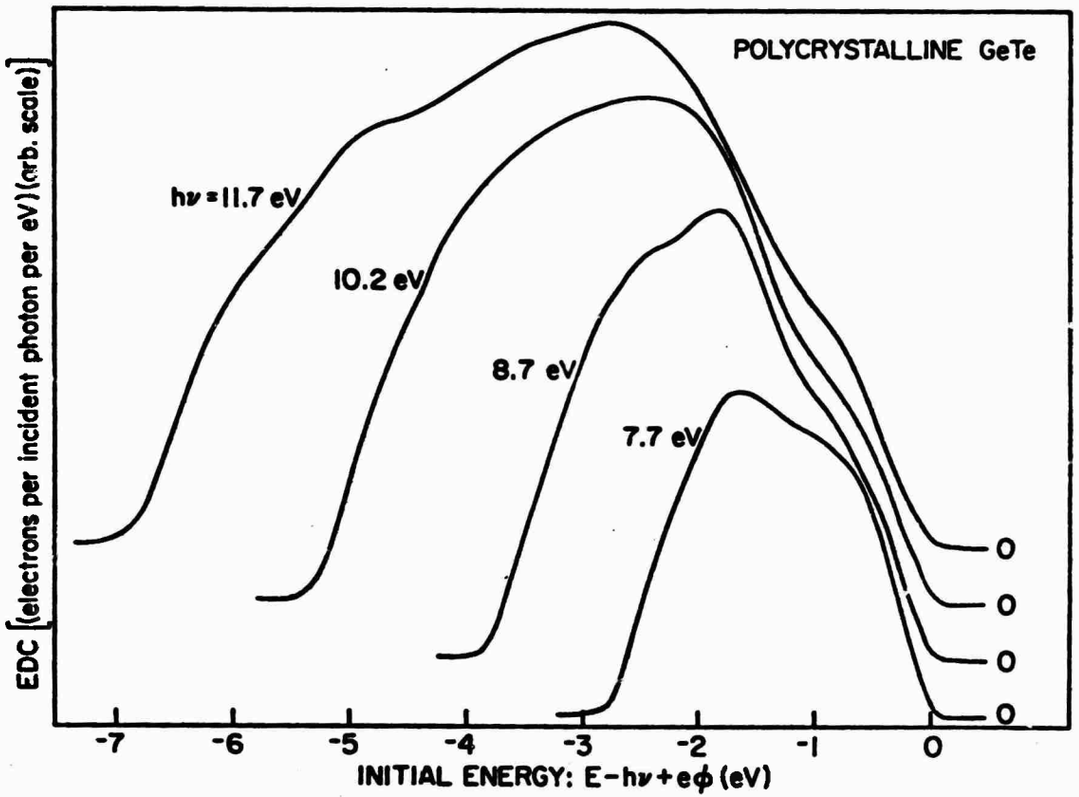

Fig. 15. Unnormalized EDCs from an Annealed Polycrystalline Film of GeTe.

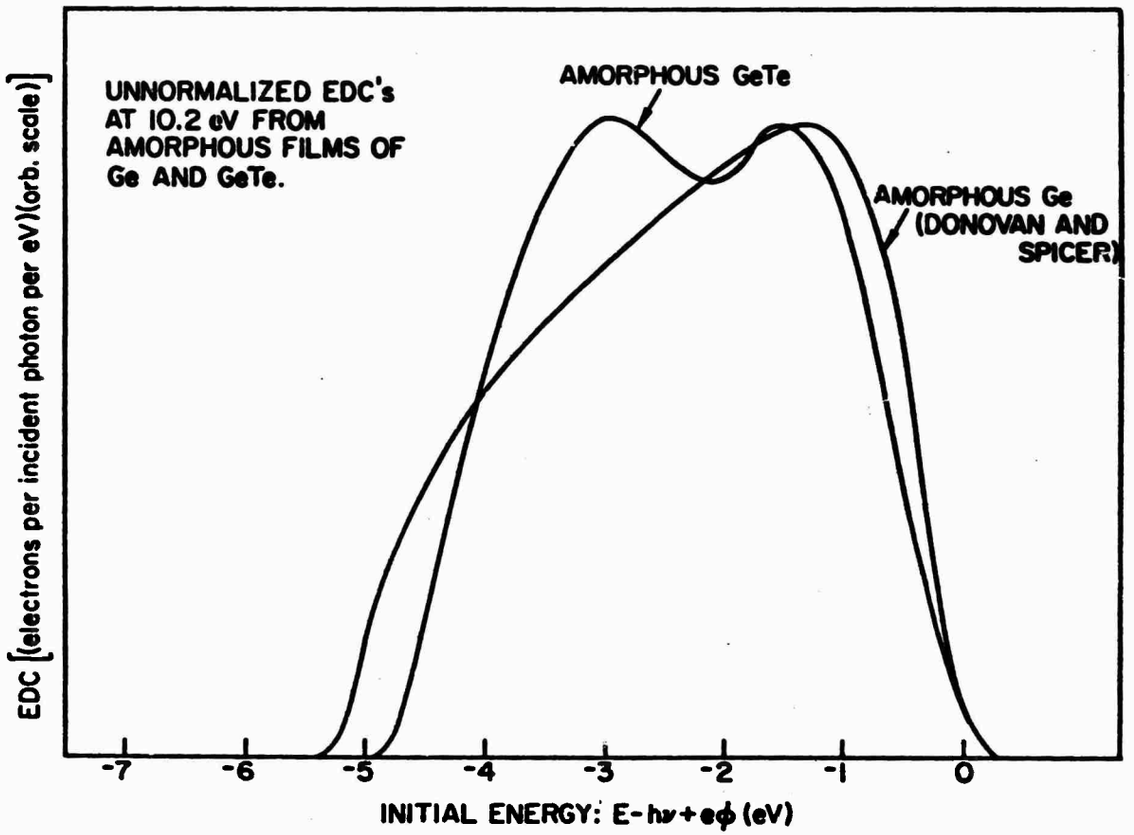

Fig. 16. Unnormalized EDCs at 10.2 eV from Amorphous Films of Ge and GeTe.

and the resulting effect on the electron states may in part explain the great difference in their EDCs.

Cesiation of an amorphous film showed no conclusive structure below the clean threshold. Above photon energies of 10.7 eV a distinct third peak does appear at the low energy end of the EDCs. However, the shift to lower energies of the second peak of the EDCs at higher photon energies and the fact that the new peak does not move with photon energy in the range examined are strong indications that the new peak consists of scattered electrons. If the threshold could be lowered significantly below the 3.6 eV value obtained at this time, another cesiation experiment would be justified.

In considering the EDCs of amorphous GeTe, it is intriguing to note that both the EDCs of amorphous Ge[4] and the present data show a peak 1.5 eV below the high energy edge. In Section I.C, we tentatively associated the peak near 1.5 eV in amorphous Ge with the covalent bond. In amorphous GeTe it appears that the Ge atoms are four-fold coordinated as in amorphous Ge, whereas the Te atoms have two bonds as in amorphous Te. Thus, one might tentatively associate the GeTe peak near -1.5 eV with a Ge bond and the peak near -3 eV with the Te bond. This model is obviously oversimplified. For example, it does not distinguish between Ge atoms bonded to Te atoms and Ge atoms bonded to Ge atoms. However, it seems a useful starting point for future investigations.

Some care has been taken to insure that the films we have examined are indeed GeTe. Microprobe analysis (spot size ~1 μ) of the sample shows a uniform composition of 50% atomic Ge and 50% atomic Te within 0.5%. The annealed film shows the characteristic peaks of crystalline GeTe in x-ray diffraction with no Ge or Te peaks present. Unheated films

appear amorphous since they show no peaks at all. Furthermore, transmission electron microscopy with a resolution capability of at least 50 Å was done on samples (~600 Å thick) evaporated under the same conditions as the films studied. There was no sign of phase separation and the very few crystallites present (less than 0.1% by volume) were each approximately one micron in diameter. Thus far it would seem reasonable to say that GeTe does evaporate as a molecular beam[5] and forms consistently reproducible thin films of GeTe.

Currently experiments on the ultraviolet reflectivity of amorphous and polycrystalline GeTe are being completed. Together with the photoemission results, these data will allow for the calculation of a density of states in at least the amorphous material.

1. J. M. Ballantyne, private communication.

2. A. Bienenstock, F. Betts and S. R. Ovshinsky, J. Non-Crystl. Solids 2, 347 (1970).

3. F. Betts, A. Bienenstock and S. R. Ovshinsky, J. Non-Crystl. Solids 4, 554 (1970).

4. T. M. Donovan and W. E. Spicer, Phys. Rev. Letters 21, 1572 (1968).

5. W. E. Howard and R. Tsu, Phys. Rev. B1, 4709 (1970).

G. Photoemission Work on As_2Se_3 and Se (R. Powell and W. Spicer)

Photoemission studies of As_2Se_3 are planned over a wide range of photon energies and temperatures. Both materials will be investigated in the amorphous and crystalline states. In addition, to better understand the nature of electrical conduction in the amorphous state, the effects of Group II dopants (e.g., Cu) on the electronic band structure will be studied. For this work, a high vacuum system has been built which is capable of reaching pressure of approximately 10^{-12} torr and which has the high pumping speed needed during the sample evaporation. The photoemission flange is now under construction.

H. Radial Distribution Studies of Si-Te Alloys (K. Connell and A. Bienenstock)

As stated above, one of the most striking features of the Ge-Te alloy radial distributions is that amorphous and crystalline GeTe short range orders are quite different. That is, amorphous GeTe shows a small coordination number and interatomic distances typical of the covalent radii. Crystalline GeTe, on the other hand, shows significantly longer nearest neighbor distances and higher coordination. Since this difference between the amorphous and crystalline short range orders is so unusual in nature, tends to eliminate the possibility of a microcrystalline model for the material and also forms the major experimental evidence of the validity of the Mott-CFO structural model, it seemed important to determine whether the difference is unique to this particular system.

To determine this, it was decided to perform radial distribution studies of amorphous and crystalline Si-Te alloys in the composition range $SiTe_2$ to Si_2Te_3. The nature of the stable crystalline form in this portion of the Si-Te phase diagram is still in dispute. Nevertheless, there is considerable evidence which indicates that the bonding is far from that expected from the Mott-CFO model and that the Si-Te nearest neighbor distance is over 3 Å, which is considerably larger than the sum of the covalent radii (2.6 Å). Hence, the appearance of a more covalent arrangement in the amorphous materials would add more justification for that model.

Initial work has been performed on amorphous $SiTe_2$. Samples for the radial distribution study were supplied by J. de Neufville of Energy Conversion Devices, Inc. These consisted of sputtered films approximately 60 microns thick. X-ray diffraction intensity data were measured and

analyzed. The resulting radial distribution is shown in Fig. 17. As can be seen from the strong oscillations at small r values, this radial distribution is not of sufficient quality for publication. Nevertheless, the peak at approximately 2.6 A is expected to remain essentially unchanged as the radial distribution itself is improved. This distance is almost exactly the sum of the SiTe covalent radii and much smaller than the 3.04 Å Si-Te distance proposed for the crystalline material. Hence, we anticipate that an improved radial distribution will show covalent bonding and small coordinations in this amorphous material. In addition, it should be noted that the second peak occurs at approximately 4.1 A. If this peak is assumed to correspond to Te-Te next nearest neighbors, then the ratio of the first neighbor peak position to the second neighbor peak position is exactly that appropriate for tetrahedra of Te containing Si atoms at their centers. Thus, crude as it is, this radial distribution presents strong evidence for a structure in which each Si atom sits at the center of a tetrahedron formed of Te atoms. That is, the structure is quite similar to that of amorphous SiO_2. Hence, there is now good reason to believe that the Mott-CFO structural model is a generally valid picture for the chalcogenide amorphous materials and that it holds even for those materials which cannot be described in that manner when they are crystalline.

Work is now under way to improve the quality of this radial distribution. Another set of x-ray intensities are being measured and the radial distribution will be recomputed. In addition, radial distributions will be evaluated for the composition Si_2Te_3 and for the corresponding crystalline forms so that existing ambiguities in the literature will not prevent us from interpreting the differences or relationships between the crystalline and amorphous structures.

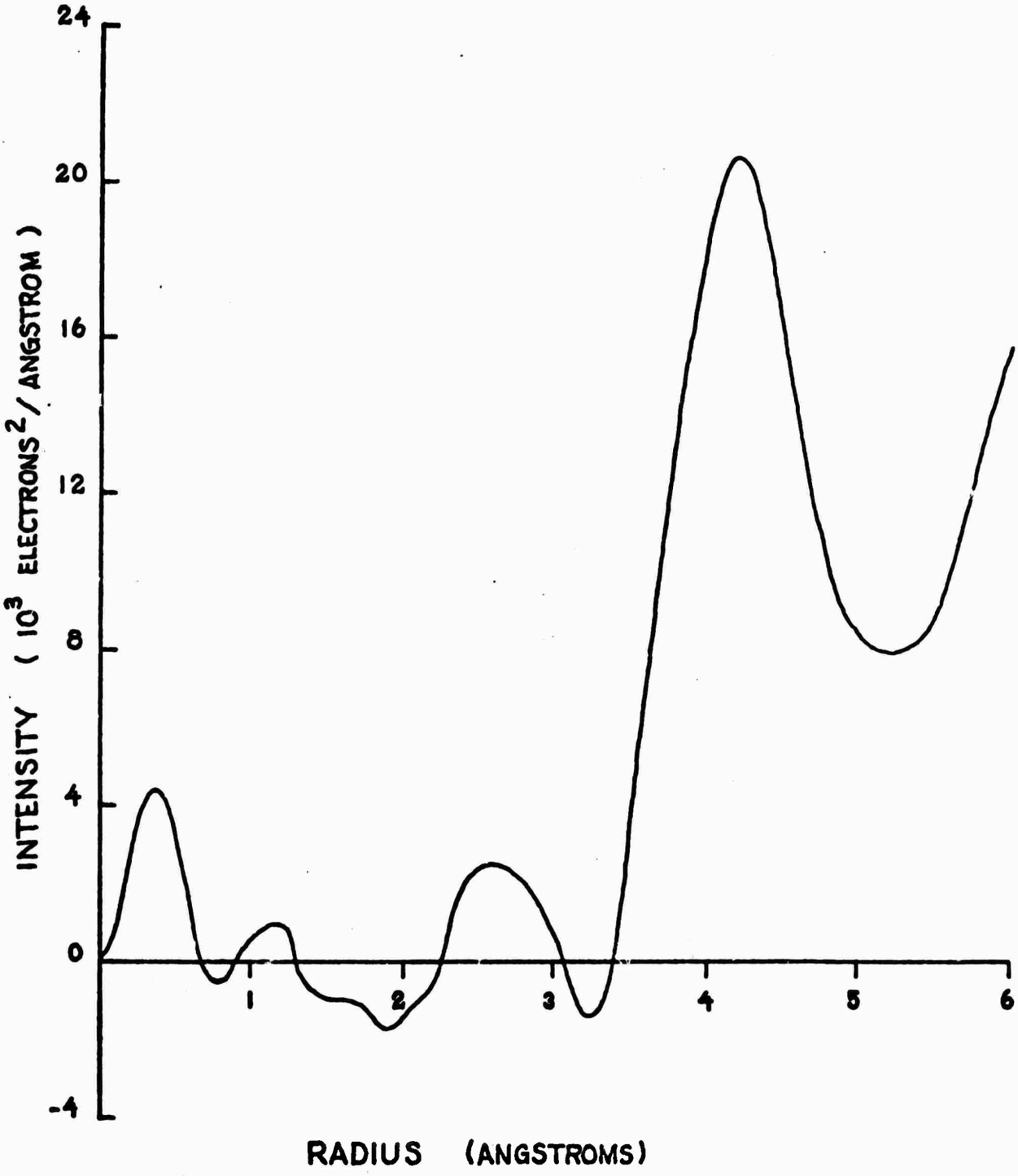

Figure 17. Preliminary radial distribution function for $SiTe_2$.


BLANK PAGE

III. MORE COMPLEX SYSTEMS

In Section III, more complex systems closely related to technological application are discussed. In the first subsection, work on the role of Group II metals in preventing the oxidation degradation of the infrared transmission properties of As_2Se_3 is described. In the second subsection, the fruits of efforts to understand photoconductivity in complex chalcogenide glasses are presented.

A. Impurity Effects in As_2Se_3 (K. Liang and A. Bienenstock)

As indicated in the original proposal, it was our intention to assess the possibility of using local mode infrared spectroscopy to understand the role of Be and Mg impurities in the conductivity of As_2Se_3. These impurities were chosen for study because of their very small modification of As_2Se_3's conductivity. This small modification is quite different from the large modification resulting from the addition of Cu.

Our initial work on these materials centered around samples which had been prepared approximately a year earlier and which had been sitting in air during the intervening period. The samples were bulk glasses of "pure" As_2Se_3, as well as bulk glasses which contained 5 or 10% additions of Be, Mg, Ca, Zn and Cu. The samples were polished to a form suitable for infrared absorption measurements.

The absorption spectrum from the "pure" As_2Se_3 sample is shown in Fig. 18. Three strong absorption peaks, at 475, 635 and 780 cm^{-1}, are evident. These peaks are similar to those obtained by Vasko et al[1] in their study of the effect of oxygen on the absorption spectrum. These authors associate the two high frequency peaks (635 and 780 cm^{-1}) with the presence of oxygen impurities, while the 475 cm^{-1} peak is apparently associated with pure As_2Se_3.

Also shown on Fig. 18 is the absorption spectrum of a sample with 5% Be. The most important feature of this spectrum is the absence of the 635 and 780 cm^{-1} peaks. Similar results are obtained through the addition of 5% Mg or Ca. These results indicate that Group II metals can be used to prevent the degradation of the As_2Se_3 infrared transmission characteristics by oxygen.

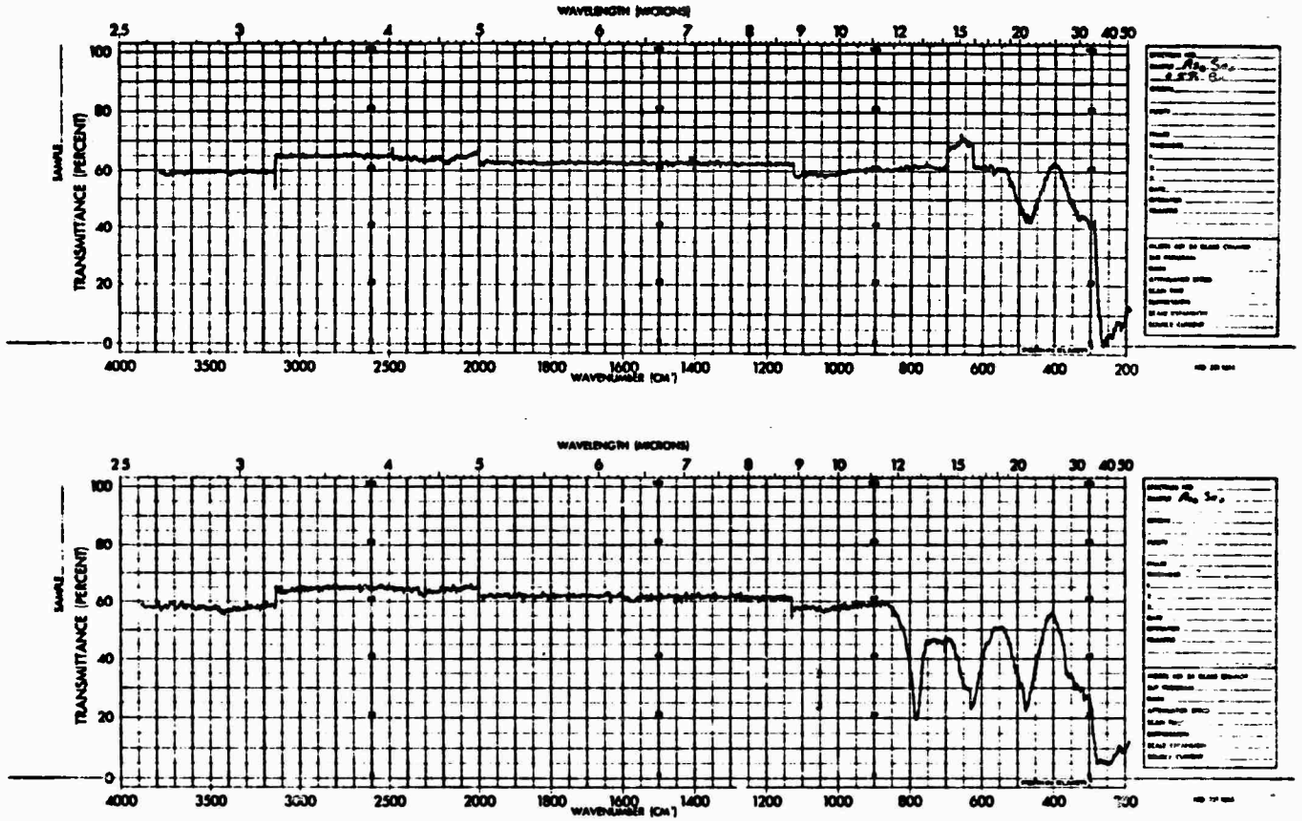

Figure 18. Infrared absorption spectrum of (top) As_2Se_3+5% Be and (bottom) "pure" As_2Se_3.

A similar type of result has been obtained by LaCourse et al[2] who studied the effect of oxygen on the infrared absorption of amorphous Se. They find that oxygen in the pure Se introduces new absorption peaks, while the addition of many metals suppresses the new oxygen peaks. These results are technologically important because they may point the way to a method of preventing oxygen degradation of infrared windows. The fact that such suppression takes place in both Se and As_2Se_3 indicates that the phenomenon is probably general and applicable to existing infrared window materials. Indeed, it may facilitate the fabrication of large windows, where high vacuum techniques are cumbersome and where the oxidation absorption peaks prevent use of the material in other than the deoxidized form.

For this reason, emphasis in this program has shifted away from the original objective. It is now our intention to systematically study the role of metallic additives in the infrared absorption properties of pure and oxidized chalcogenide glasses. Towards this end, we are constructing a high vacuum glass preparation system so that the oxidation of the samples can be controlled and so that large numbers of samples can be prepared. This construction is essentially completed and the system will soon be tested.

At the same time, we are aware that any improvements in resistance to oxidation degradation achieved by such metallic additions might be counterbalanced by compensating decreases in the quality of other properties. For this reason, we have decided to examine the softening temperatures of these materials through DTA measurements. While such a program must await completion of the sample preparation equipment, we have made preliminary studies on the old materials. These indicate a very slight

(1-5°C) shift downward of the softening temperature. This should not be of technological importance. On the other hand, the same studies indicate that the crystallization rate increases markedly at approximately 310°C. To be more precise, the DTA studies performed at a 20°C/min heating rate show the beginning of a crystallization exotherm at 310°C in the 5% Mg sample. The exotherm peak is at approximately 325°C. A similar DTA study of the "pure" As_2Se_3 shows no such exotherm. These studies will be extended when the sample preparation equipment construction is completed.

Finally, we should note that this suppression of oxidation degradation is not obtained through the addition of all metals. Figure 19 shows the absorption spectrum obtained from a sample containing 10% Cu. It is apparent that the oxidation peaks are present. Attempts to understand why some metals do and other metals do not suppress the oxidation degradation will be undertaken. In addition, we shall attempt to determine if the addition of metals suppresses only the initial degradation associated with oxygen in the melt or also suppresses subsequent oxidation in the atmosphere at elevated temperatures. Finally, we shall attempt to understand why the metallic additions increase the crystallization rate.

1. A. Vasko, D. Lezal and I. Srb, J. Non-Cryst. Solids 4, 311 (1970).

2. W. C. LaCourse, V. A. Twaddell and J. D. Mackenzie, J. Non-Cryst. Solids 3, 234 (1970).

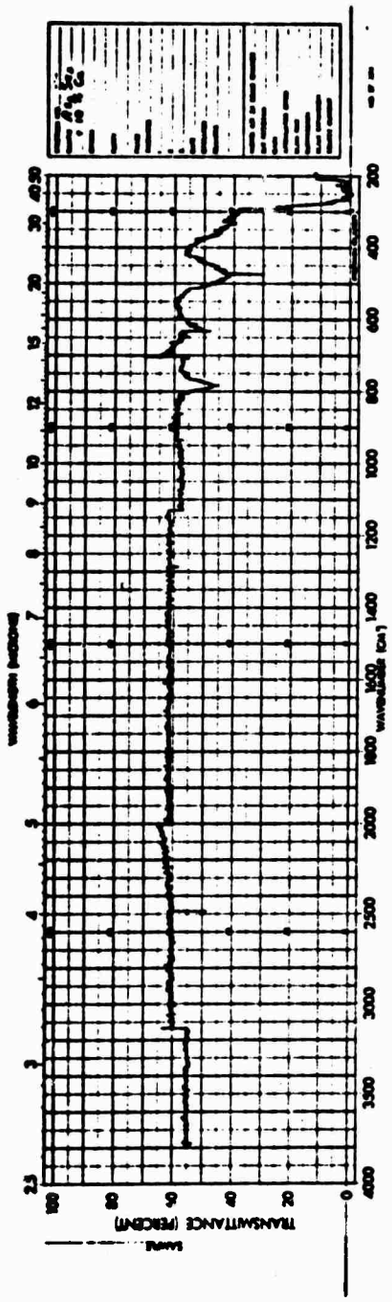

Figure 19. Infrared absorption spectrum of As_2Se_3+10% Cu.

B. Photoconductivity of Amorphous Chalcogenides (Richard H. Bube and Thomas C. Arnoldussen)

1. Theoretical Program

A model for photoconductivity has been developed for amorphous chalcogenide alloys which is able to describe many of the characteristic properties of these materials and to provide a means of determining the characteristic parameters of localized or partially localized states. The critical feature of the model, arrived at by consideration of many possibilities in comparison with actual data, is a high density of effective recombination states located within an energy E^* of each band edge, the energy E^* having a value between about 0.1 and 0.3 eV for different materials investigated. The model describes appropriately the variation of photoconductivity with excitation intensity at different temperatures, the variation of photoconductivity with temperature at different light intensities, and the shift in the temperature for maximum photoconductivity with excitation intensity. Additional data to which the model can be profitably related are those derived from measurements of thermoelectric power and thermally stimulated conductivity. A paper describing the model is to be presented at the International Conference on Amorphous and Liquid Semiconductors, to be held at the University of Michigan in August 1971.

a. Photoconductivity Characteristics

Data on the temperature and excitation intensity dependence of photoconductivity in amorphous chalcogenides are available from the work of E. Fagen at Energy Conversion Devices, Inc. The materials used for comparison are $Ge_{15}Te_{81}Sb_2S_2$ (Material A), $Si_{11}Ge_{11}As_{35}P_3Te_{40}$ (Material B), and $Ge_{16}As_{35}Te_{28}S_{21}$ (Material C).

Typical photoconductivity curves for these materials are represented in Fig. 20 in order to illustrate the major characteristics of the behavior.

(a) In the high-temperature region I, the photoconductivity is smaller than the dark conductivity, varies linearly with excitation intensity, and increases exponentially with 1/T.

(b) In the intermediate region II, the photoconductivity becomes greater than the dark conductivity, varies as the square-root of the excitation intensity, and decreases exponentially with 1/T.

(c) Between regions I and II, the photoconductivity reaches a maximum at T_{max}. The value of T_{max} shifts with excitation intensity.

(d) In the low-temperature region III, the photoconductivity is much greater than the dark conductivity, varies linearly with excitation intensity, and appears to approach an almost constant asymptotic value at very low temperatures.

Any successful model must reproduce these characteristics in a qualitative way, and must in addition provide the means of deducing information about the localized states in the amorphous material in a quantitative way.

b. Summary of Model

We assume that non-localized states exist for energies greater than a conduction mobility edge and less than a valence mobility edge. For energies between these two edges, we assume a continuous distribution of localized or partially-localized states, extending from each mobility edge into the mobility gap.

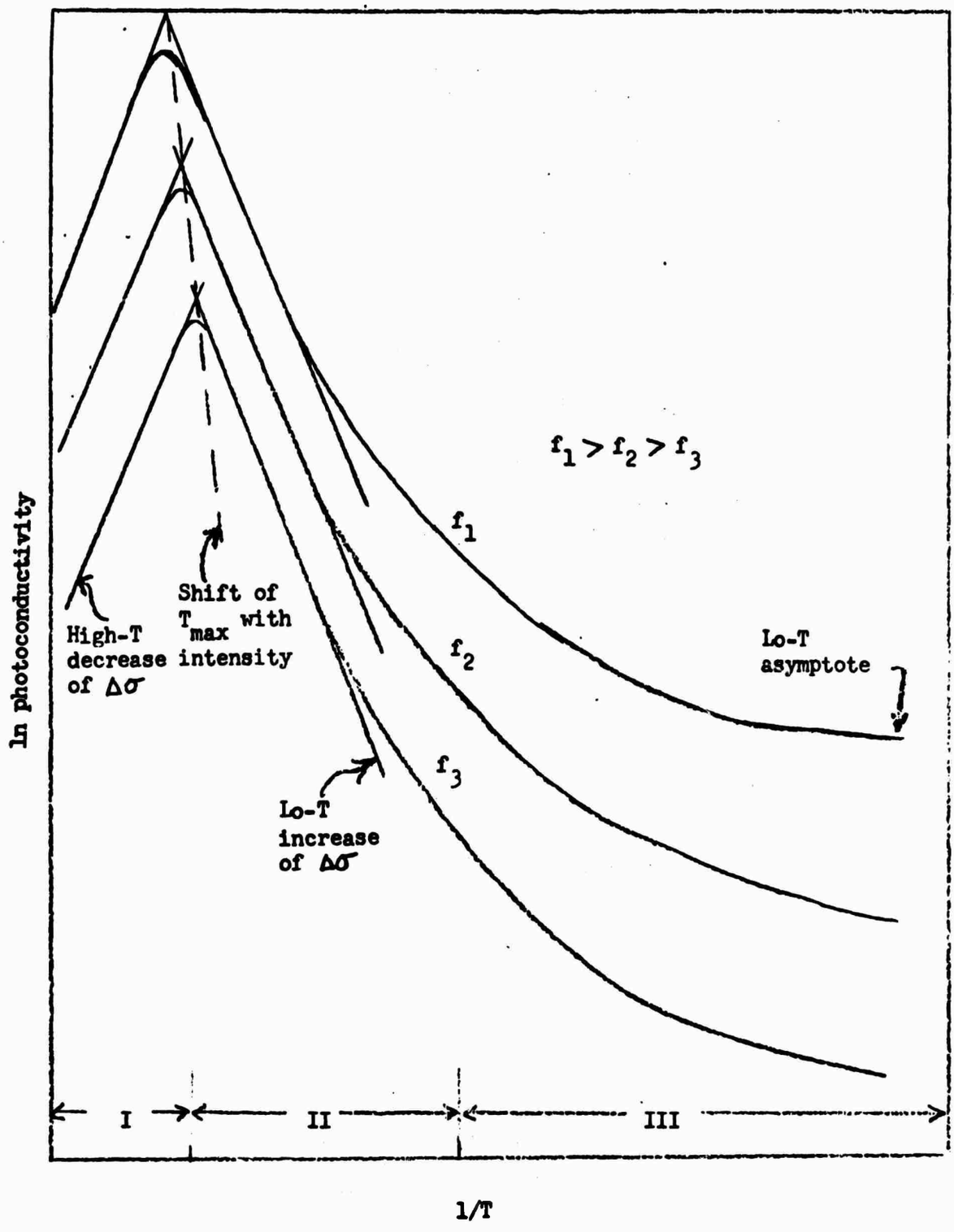

Figure 20. Typical variation of photoconductivity with excitation intensity, f, and temperature, T, for an amorphous chalcogenide.

The procedure for the calculation of carrier density as a function of excitation intensity and temperature is as follows.

(1) Consider a specific level in the distribution of localized states. By considering the steady-state conditions for the occupancy of this level as affected by thermal excitation to each band, recombination from each band, and recombination from upper localized levels to lower localized levels, derive an expression for the occupancy of this specific level.

(2) By considering the steady-state conditions for the density of free carriers in terms of the integrated contributions of specific levels from (1), calculate the desired variation of free carrier density on excitation intensity and temperature.

If one starts with a perfectly general distribution of localized states in the forbidden gap, it soon becomes clear that a region in which the carrier density decreases exponentially with $1/T$ (Region II) occurs only if the density of effective recombination centers is limited to regions lying E^* from each band edge. The density of these effective recombination centers (the product of density of states and capture coefficient) must fall off with increasing E past E^* away from the band edge more rapidly than the Boltzmann factor in order to give the observed Region II behavior.

To date we have carried out the development of the model in detail for the case in which only recombination from non-localized to localized states need be considered, and for the case in which both this recombination mode and the recombination mode involving direct localized-localized recombination is considered. We have also carried out the development of the model for symmetric localized state distributions and

for asymmetric localized state distributions. Although it proves possible to describe all the photoconductivity data without including localized-localized recombination, it does not appear possible to include also the dark conductivity behavior in a single consistent representation. If, however, on self-consistent grounds one treats the high-temperature behavior of Region I as being dominated by non-localized to localized recombination, but the behavior of Regions II and III as being dominated by localized-localized recombination, it is possible to present a complete consistent description of all photoconductivity and dark conductivity data.

c. Specific Results for Symmetric Model

As an illustration of the specific results, we describe here the expressions for the symmetric form of the model described at the end of the last section, for which a consistent picture can be made.

In the high-temperature Region I,

$$\Delta p = \frac{f\, e^{-b/2k}}{4\beta^{o} N_E (1/\gamma)\, kT} \exp\left[\frac{(E_{Go} - 2E^*)}{2kT}\right] \qquad (1)$$

where Δp is the photoexcited carrier density, f is the excitation intensity, b is the temperature coefficient of the bandgap,

$$E_G = E_{Go} - bT \ ,$$

β^{o} is the capture coefficient of a neutral localized state, N_E is the density of localized states within E^* of the band edges, γ is the ratio of the capture coefficient of a neutral localized state to a charged localized state.

In the intermediate-temperature Region II,

$$\Delta p = \frac{N_c}{2N_E kT}\left(\frac{f}{K}\right)^{1/2} \exp\left[-\frac{E^*}{kT}\right] \qquad (2)$$

where N_c is the effective density of non-localized states, and K is the recombination coefficient for localized-localized recombination.

Setting Eqs. (1) and (2) equal permits a description of the variation of T_{max} with f and E_G.

$$\frac{1}{kT_{max}} = -\frac{\ln\left[f/N_c^2\right]}{E_{Go}} + \frac{\ln\left[\dfrac{\beta^{o^2}(1/\gamma)^2 e^{b/k}}{K}\right]}{E_{Go}} \qquad (3)$$

The dark equilibrium carrier density is proportional to $\exp(-E_{Go}/2kT)$.

In applying these results to the general situation, it is necessary to assume that there may be a temperature dependent mobility of the form

$$\mu = \mu_o \exp(-E'/kT) \qquad (4)$$

Analysis of a particular set of experimental data in terms of the model then proceeds as follows.

1. Since the activation energy for the dark conductivity is $[(E_{Go}/2) + E']$, and E_{Go} can be determined directly from the intensity dependence of T_{max} after Eq. (3), these two pieces of information can be used to determine E_{Go} and E'.

2. Since the activation energy for the Region II variation of photoconductivity with temperature is $[E^* + E']$, E^* can be determined. The values of E_{Go}, E^*, and E' determined in this way should now be consistent through Eq. (1) with the activation energy for Region I.

3. The evaluation of other parameters of the system can be made through the second term in Eq. (3) and the theoretical expression for the low-temperature limiting value.

d. Quantitative Example

In order to illustrate the way in which the model can be applied quantitatively, consider actual data for a specific excitation intensity for Material A.

There are a total of 11 parameters: E_{Go}, E^*, E', b, N_c, N_E, β^o, γ, K, μ_o and $\mu_{77}o$. Here the last quantity recognizes the fact that for agreement with experimental data, the thermally activated behavior of the mobility must give way to a much slower temperature dependence at very low temperatures. There are 8 equations which can be brought to bear to evaluate these parameters. This means that 3 parameters must either be chosen arbitrarily or evaluated independently. Here we may take $b = 4 \times 10^{-4}$ eV/o, as a reasonable estimate from other known data on the shift of the optical absorption edge in these materials with temperature; $\beta^o = 10^{-9}$ cm^3/sec, as a kind of classical value for a neutral center; and $\mu_o = 20$ cm^2/V-sec as a reasonable estimate.

The following values are deduced:

$$E_{Go} = 0.72 \text{ eV}$$

$$E^* = 0.11 \text{ eV}$$

$$E' \simeq 0.08 \text{ eV}$$

$$\gamma = 10^{-3}$$

$$\mu_{77}^{o} = 0.009 \text{ cm}^2/\text{V-sec}$$

$$N_c = 1.1 \times 10^{19} \text{ cm}^{-3}$$

$$K = 2.4 \times 10^{-6} \text{ cm}^3/\text{sec}$$

$$N_E = 3.3 \times 10^{18} \text{ cm}^{-3} \text{ eV}^{-1}$$

It is our intention to refine the model further, apply it to as many sets of data as are currently available to us, and utilize it as far as possible as an aid in the interpretation of photoconductivity data on materials to be prepared by us as part of this program, as described in the following section.

2. Experimental Program

The experimental work in which we are engaged is the investigation of the electrical properties of amorphous chalcogenide alloys of the generic type used in switching. We plan to measure the dark and photoconductivity as a function of temperature, light intensity and wavelength; the optical absorption in the near and far infrared, noting the shift in optical energy gap with temperature; the drift and conductivity mobilities, if possible; the photoconductivity decay and the thermally stimulated conductivity; and finally the thermoelectric power on those samples with a moderately low resistivity.

a. Materials

We are investigating the following alloy compositions both in thin film and bulk (wherever bulk glassy samples of a given composition are possible) forms.

$$\left[Ge(Se_yTe_{1-y})_2\right]_x \left[As_2(Se_yTe_{1-y})_3\right]_{1-x}$$

where x takes on values 0, 1/4, 1/2, 3/4, and 1; and y takes on values 1/3 and 2/3.

The reasons for choosing such a group of materials are the following.

(1) We wish to study amorphous chalcogenide alloys of the switching type, which have component elements from groups IV, V, and VI of the periodic table.

(2) With a possible working model for the conduction mechanism and density of states for amorphous chalcogenide alloys, it is very desirable to observe how the model's parameters vary with composition.

(3) We can simplify the compositional variation by choosing a pseudo-binary series of compositions, e.g., Ge-Se bonds being distinct from As-Se bonds. We maintain the stoichiometric ratios $GeSe_2$ and As_2Se_3 in which all bonds are single and hypothetically saturated. Moreover we would expect that there would be few Ge-Ge, Se-Se, As-As, As-Ge bonds. All these same things could be said of compositions using Te in place of Se.

(4) For convenience and feasibility of measurements, it is desirable to look at moderately high and low resistivity samples rather than very high or low resistivity samples. For this reason we use a fixed ratio of selenium to tellurium rather

than Se or Te alone. This preserves the binary aspect from the standpoint that we still have group IV-V bonds and V-VI bonds. However, since Se bonds have a different energy from Te bonds, we have introduced a complication which makes this a quaternary system. In order to obtain some idea of the effect of replacing Se by Te, we plan to investigate at least two series of compositions, each with a different fixed ratio of Se:Te. The ratios 1:2 and 2:1 should also enable us to look at both bulk and thin films for most compositions.

b. Sample Preparation

The preparation of both bulk and thin film samples begins with the loading of a measured composition of the constituent elements into a quartz ampule which is evacuated to about 10^{-5} Torr and sealed. This ampule is then fired at about 800°C for four to five hours in a rocking furnace to assure adequate mixing. The ampule is removed from the furnace and immediately quenched in a water bath.

At this stage a portion of the sample is removed and subjected to x-ray examination to determine whether or not it is amorphous. If the quenched material is indeed glassy, it is suitable for making bulk measurements. If bulk samples are to be used, the larger chunks are polished and shaped, and where desired sandwich or interdigital electrodes are deposited by sputtering molybdenum through a mask.

If thin film samples are to be made, the next step after quenching the bulk material is to prepare a sputtering cathode. The quenched bulk (whether or not it is glassy) is ball milled to a powder of mesh about 1 micron or less. This powder is then hot-pressed in a 3/4 inch die to form the sputtering cathode. No thin films have yet

been prepared since we are awaiting the arrival of a glove box, as well as a hot press and ball mill which will fit in the glove box. The glove box is needed because the ball milling and hot pressing should be performed under an inert atmosphere to prevent oxidation at the elevated temperatures.

Basically four types of thin film samples are anticipated: (1) various thickness samples without electrodes for near infrared optical absorption measurements; (2) thicker, narrow samples with end electrodes for thermoelectric power measurements on the higher conductivity samples; (3) interdigital electrodes for dark and photoconductivity measurements, as well as photoconductivity decay and thermally stimulated current measurements; (4) sandwich electrodes for drift mobility experiments on the higher resistivity samples. In this last case the device structure is somewhat more complicated than in the other samples. First, a metallic substrate is used. A submicron film of SiO_2 is deposited on the metal substrate and the active film is sputtered on top of the SiO_2. Then another submicron film of SiO_2 is deposited followed by a 1000 Å or less film of aluminum (or other metal which exhibits good transparency to the electron beam used in performing the drift mobility experiment). The SiO_2 insulator films serve to prevent electron and hole injection from the electrodes so that all the carriers injected into the sample are due to the electron-hole pairs generated by the electron beam at the upper transparent electrode.

The thinner samples of this type show more promise in measuring the drift mobility, but may exhibit capacitance complications. On the thicker samples, it is less likely that we will be able to measure the carrier transit time and hence the drift mobility, but because the

capacitance should be less troublesome we should have a good chance of measuring accurately the initial value of the current transient from which the conductivity mobility may be obtained.